

Benign Overparameterization in Membership Inference with Early Stopping

Jasper Tan, Daniel LeJeune, Blake Mason, Hamid Javadi, Richard G. Baraniuk
Department of Electrical and Computer Engineering
Rice University

Abstract

Does a neural network’s privacy have to be at odds with its accuracy? In this work, we study the effects the number of training epochs and parameters have on a neural network’s vulnerability to membership inference (MI) attacks, which aim to extract potentially private information about the training data. We first demonstrate how the number of training epochs and parameters individually induce a privacy–utility trade-off: more of either improves generalization performance at the expense of lower privacy. However, remarkably, we also show that jointly tuning both can eliminate this privacy–utility trade-off. Specifically, with careful tuning of the number of training epochs, more overparameterization can *increase model privacy* for fixed generalization error. To better understand these phenomena theoretically, we develop a powerful new leave-one-out analysis tool to study the asymptotic behavior of linear classifiers and apply it to characterize the sample-specific loss threshold MI attack in high-dimensional logistic regression. For practitioners, we introduce a low-overhead procedure to estimate MI risk and tune the number of training epochs to guard against MI attacks.

1 Introduction

Two fundamental decisions for any machine learning system designer are (a) how many model parameters to use and (b) how long to train those parameters (number of training epochs). These two choices have been an active area of research for many years and have given rise to popular machine learning design principles such as early stopping [1, 2] and pruning [3], as well as theoretical guides such as the VC dimension [4]. For modern deep neural networks (NNs), the conclusion of recent research is that increasing both the number of parameters and the number of epochs generally aids the generalization performance of networks [5]. This phenomenon has been termed double descent [6] (both parameter-wise and epoch-wise [5]) and benign overfitting [7] and suggests that machine learning system designers should opt for the largest possible model trained for as long as possible in order to maximize its performance on unseen data.

However, when training machine learning models on sensitive data [8–10], it is crucial to understand the attendant privacy issues to prevent data leaks. Alarming, multiple attacks have been developed in the literature to perform *membership inference* (MI), which extracts information about specific examples in a model’s training dataset even given only black-box access [11–13]. Without a firm understanding of what properties of a model yield such privacy vulnerabilities, there always exists the threat that a large-scale model trained on sensitive user data will be susceptible to such an attack and leak large amounts of private data.

Therefore, the modern machine learning system designer needs to know the answer to the following foundational question: **how do the number of parameters and the number of training epochs affect the privacy of a machine learning model, and is tuning them for privacy at odds with generalization?** In this paper, we study this question from the perspective of MI.

Empirically, we study the effect on MI of the number of parameters of a NN and the number of training epochs in binary feature classification, image classification, and language translation. As our system designer might fear, although past works such as [5] have shown that increasing the number of parameters or training epochs decreases a model’s generalization error, we demonstrate that it also *increases* the model’s vulnerability to MI attacks. In sum, we expose new **privacy–utility trade-offs inherent to NNs** as a function of either the number of parameters or the number of training epochs.

Theoretically, we study the privacy–utility trade-off via a novel leave-one-out analysis of high-dimensional logistic regression. Our analysis provides a precise asymptotic characterization of MI for the powerful sample-specific loss thresholding attack [14] and demonstrates that the same privacy–utility trade-offs exist in settings such as overparameterized linear classification, which is known to exhibit benign overfitting as the number of parameters increases [15–17].

Remarkably, however, both our empirical and theoretical analyses demonstrate that, despite the presence of the privacy–utility trade-off as a function of the number of parameters or training epochs *individually*, if we carefully tune them *jointly* by decreasing the number of training epochs as we increase width, then there is no privacy–utility trade-off. In particular, if the number of training epochs is tuned to achieve a fixed privacy level, then increasing the number of parameters (by increasing a NN’s width) only increases the model’s test accuracy.

For the system designer, our analyses provide a clear recommendation for how to achieve a high degree of both privacy and utility: opt for a wider NN while carefully performing early stopping to achieve the desired balance between privacy and utility. In summary, our paper has three core contributions:

1. We demonstrate how individually increasing either the number of parameters or the number of training epochs of a classification model **decreases the model’s privacy**.
2. We discover that wider NNs enjoy an improved privacy–utility trade-off compared to narrow ones, and that, controlling for the privacy level by early stopping, **increased generalization performance due to overparameterization is not at odds with privacy**. For practitioners, we provide a lightweight procedure to perform early stopping given a privacy budget.
3. We theoretically analyze high-dimensional logistic regression and replicate our empirical NN observations for a bi-level feature ensemble using a **novel leave-one-out analysis that may be of independent interest**. In the process, we prove a fundamental MI vulnerability for overparameterized logistic regression models.

Related work. There is a wealth of research in privacy and machine learning. This work contributes to the rapidly growing field of membership inference (MI). We refer the reader to [18, 14] for a comprehensive summary of the prior art in MI. We mention a few works that are especially relevant for our work. [13] show that given the individual prediction values for each class, it is possible to perform MI by leveraging shadow models with the same architecture as the true model. [19] show that this type of attack can be performed using only the scalar loss value and present optimality results for such attacks. This is similar to confidence-based attacks as in [20, 21]. [22–27] all study how various types of regularization can defend against MI attacks. Furthermore, MI is a special case of differential privacy (DP), and we refer the reader to [28] and [29] for a survey of DP results and its connections to deep learning, respectively, as well as to [30] for a precise connection between DP and MI. Whereas works such as [31, 32] propose alternate losses and training procedures to preserve DP, in this work we analyze how properties of ordinary networks and training, such as the number of parameters number of training epochs, directly relate to MI. The astute reader may expect some form of a link between MI and these properties, as works such as [33] establish worst case bounds on DP as a function of the dimension of the data, though this is not tied to any particular learning algorithm.

In this paper, we are interested in understanding both empirically and theoretically how overparameterization affects MI in classification. [25, 34] show that pruning a network can improve MI robustness. [27] show empirically that MI tends to be easier on more challenging learning tasks. [30] study the theoretical connection between overfitting and membership advantage but do not connect this to properties of ML models such as the number of parameters of a neural network, the number of training epochs, or the dimension of a linear model. [22] present theory connecting the dimension of a Gaussian linear model to its vulnerability to MI attacks in regression tasks.

We wish to study the trade-off between vulnerability to MI attacks and strong generalization behavior in classification. [5] demonstrate double descent behavior in neural networks as a function of the number of parameters and number of training epochs. In the particular case of language models, [35] propose a privacy-preserving fine-tuning strategy and show empirically that larger models tend to outperform smaller ones when both achieve the same level of privacy. The most similar work to ours is that of [22], who present

Pareto curves for MI accuracy versus mean squared error in linear regression by adopting a similar model as was used by [7] to demonstrate benign overfitting. To theoretically understand the trade-off between generalization error and an adversary’s MI accuracy, we study the popular “bi-level ensemble” model that has been shown to exhibit benign overfitting in classification [15, 16]. To characterize the difference of predictions on training points and test points, we leverage the proportional asymptotics regime, where precise analysis is enabled by tools such as the convex Gaussian min-max theorem [36] and approximate message passing [37–39]. In particular, we build upon [40] to analyze the behavior of logistic regression in the asymptotic regime.

2 Theoretical foundations of membership inference

We define our MI problem for classification as follows. Let $\mathcal{S} = ((\mathbf{x}_i, y_i))_{i=1}^n$ be a training dataset of features $\mathbf{x}_i \in \mathcal{X} \subseteq \mathbb{R}^p$ and labels $y_i \in \mathcal{Y} = \{1, \dots, k\}$ (i.e., multiclass classification). We assume that each data point and its associated label is an independent sample from a distribution \mathcal{D} over the data such that $\mathcal{S} \sim \mathcal{D}^n$. Furthermore let \mathcal{F} denote a class of machine learning models (e.g., linear models or neural networks) such that for $f \in \mathcal{F}$, $f : \mathcal{X} \rightarrow \mathbb{R}^k$, producing a vector of confidence values from which the final prediction is given as $\hat{y}(\mathbf{x}) = \arg \max_j [f(\mathbf{x})]_j$. For each pair (\mathbf{x}, y) , we have access to a loss function $\ell : \mathcal{Y} \times \mathbb{R}^k \rightarrow \mathbb{R}_{\geq 0}$ that measures the performance of any $f \in \mathcal{F}$ on the data \mathcal{S} . The model’s *test (misclassification) error* is defined as $\mathcal{E}(f) = \Pr(y \neq \hat{y}(\mathbf{x}))$, where (\mathbf{x}, y) is drawn from \mathcal{D} for our theoretical results or from the test set for our experiments. Finally, let A be a MI adversary. For a fixed model $f \in \mathcal{F}$ trained on \mathcal{S} , we assume that $A : \mathcal{F} \times \mathcal{X} \times \mathcal{Y} \rightarrow \{0, 1\}$ has access to f and a sample (\mathbf{x}, y) and predicts 1 if it believes $(\mathbf{x}, y) \in \mathcal{S}$ and 0 otherwise. To be rigorous, we define MI as the following experiment [30, 22].

Experiment 1. *Given distribution \mathcal{D} , model class \mathcal{F} , loss function ℓ , and adversary A , a membership inference experiment is*

1. *Sample $\mathcal{S} \sim \mathcal{D}^n$.*
2. *Learn $\hat{f} \in \arg \min_{f \in \mathcal{F}} \sum_{i=1}^n \ell(y_i, f(\mathbf{x}_i))$.*
3. *Sample $m \in \{0, 1\}$ uniformly at random.*
4. *If $m = 0$, sample a new test data point $(\mathbf{x}, y) \sim \mathcal{D}$. If $m = 1$, sample a training data point $(\mathbf{x}, y) \in \mathcal{S}$ uniformly at random.*
5. *Observe the adversary’s prediction $A(\hat{f}, \mathbf{x}, y) \in \{0, 1\}$.*

In essence, Experiment 1 reduces the problem of MI to one of hypothesis testing. Accordingly, we quantify the performance of an adversary in terms of its *membership (inference) advantage*, defined as the difference between the true positive rate and the false positive rate.

Definition 1 ([30]). *The membership advantage of an adversary A against \hat{f} is*

$$\text{Adv}(A) = \Pr(A(\hat{f}, \mathbf{x}, y) = 1 \mid m = 1) - \Pr(A(\hat{f}, \mathbf{x}, y) = 1 \mid m = 0), \quad (1)$$

where $\Pr(\cdot)$ is taken jointly over all randomness in Experiment 1.

Membership inference can be performed successfully when the model treats points from the training dataset \mathcal{S} “differently” than new test points. More precisely, if the distribution or other statistics of the model’s outputs on training points differs from that on new test points, then MI attacks can distinguish between the two distributions to determine if $m = 0$ or $m = 1$. A common attack is the loss threshold attack, which takes the form $A(f, \mathbf{x}, y) = \mathbb{1} \{\ell(y, f(\mathbf{x})) < \tau(\mathbf{x}, y)\}$ and has grown in popularity due to its simplicity and effectiveness [30, 19, 41]. It leverages the difference in the distributions of the model’s loss, rather than output, on training vs. new test data points. Indeed, we observe in Figure 1 that as a model trains on data, its loss on those data points decreases at a rate faster than its loss on non-training data points, enabling successful loss threshold attacks. While global loss thresholds ($\tau(\mathbf{x}, y) = \tau$ for all (\mathbf{x}, y)) are occasionally used for simplicity, it has been shown that sample-specific loss thresholds are more powerful [41, 14]. For this reason, we consider sample-specific loss thresholding adversaries for our experiments in this work.

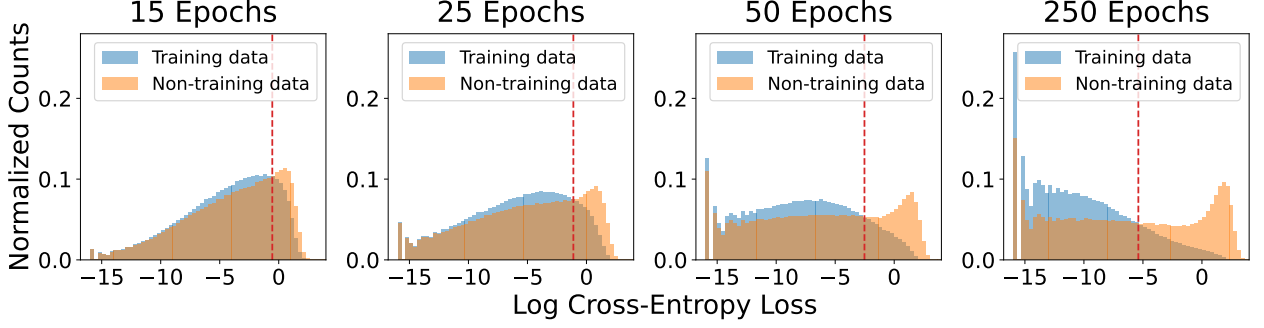


Figure 1: **Loss gap increases with epochs.** Empirical histograms of log cross-entropy losses for training and non-training data points of 20 ResNet18s ($w = 64$) trained on CIFAR10 for different training epochs. While both distributions generally shift towards smaller losses with more epochs, the losses for training points shifts at a quicker rate than those for non-training points, enabling loss-threshold attacks. The optimal threshold is depicted with the red dashed line. This also illustrates why loss threshold MI accuracy increases with epochs (Figure 4). For visualization purposes, we drop points that achieve 0 (to machine precision) loss.

2.1 Analysis framework and core theoretical result

To theoretically analyze MI, we consider a regularized high-dimensional logistic regression setting. We define the logistic loss $\ell(y, z) = \rho(z) - yz$ in terms of the function $\rho(z) = \log(1 + \exp(z))$ whose derivative $\rho'(z) = 1/(1 + \exp(-z))$ is the sigmoid function. We let $\mathbf{x}_i \sim \mathcal{N}(\mathbf{0}, \frac{1}{p}\Sigma)$ for some positive definite covariance matrix $\Sigma \in \mathbb{R}^{p \times p}$, and for ground truth coefficients $\beta^* \in \mathbb{R}^p$, binary labels $y_i \in \{0, 1\}$ are generated such that $\Pr(y_i = 1 | \mathbf{x}_i) = \rho'(\mathbf{x}_i^\top \beta^*)$. Our learned decision function is $\hat{f}(\mathbf{x}) = \mathbf{x}^\top \hat{\beta}$, yielding predictions $\hat{y}(\mathbf{x}) = \mathbb{1}\{\hat{f}(\mathbf{x}) > 0\}$, where

$$\hat{\beta} = \arg \min_{\beta} \frac{1}{n} \sum_{i=1}^n \ell(y_i, \mathbf{x}_i^\top \beta) + \frac{\lambda}{2p} \|\beta\|_2^2. \quad (2)$$

We then consider the asymptotic limit as $n, p \rightarrow \infty$ with $n/p \rightarrow \delta \in (0, \infty)$. This enables us to apply the analysis of [40], who used the convex Gaussian min-max theorem (CGMT) [36] to completely characterize the generalization performance of logistic regression in terms of the solution to a nonlinear system of equations of a few scalar variables; see Appendix B.2 for details.

The challenge in studying privacy is that we must additionally characterize the difference between the distributions of model outputs for training points and test points. Existing analyses from frameworks such as the CGMT are insufficient to give us the distributions of the outputs for a *single* training point over the randomness of the remaining training dataset, which we need in order to study the sample-specific loss thresholding adversary. Therefore, we provide a novel leave-one-out-based characterization of the distribution of the output of a linear model for any specific training point. The following result is an informal statement of a more detailed version in Appendix C.

Theorem 1 (informal version of Theorem 4). *Consider the solution $\hat{\beta}$ to the optimization problem in (2). There exists $\gamma > 0$ such that for any training point \mathbf{x}_i ,*

$$\mathbf{x}_i^\top \hat{\beta} \xrightarrow{d} \text{Prox}_{\gamma \ell(y_i, \cdot)} \left(\mathbf{x}_i^\top \hat{\beta}_{-i} \right), \quad (3)$$

where $\hat{\beta}_{-i}$ is the solution to (2) with (\mathbf{x}_i, y_i) omitted from the training set, and \xrightarrow{d} denotes convergence in distribution where the randomness is over the other $n - 1$ training points.

That is, the distribution of outputs for training points is simply the distribution of the proximal operator (defined in Appendix B.1) of the loss function applied to the output of the training point as if it was a new

test point. This will drive the loss closer to zero for training points than for new test points, and so as discussed above, an adversary can exploit this difference to perform MI.

We strongly believe this theoretical tool to be of independent interest, opening the door to future theoretical study of privacy in high dimensional linear models, in particular with sharp asymptotics for any given adversary rather than simply worst-case bounds. Our proof strategy is general and applies to general convex losses and regularization penalties, as we describe in Appendix C. A particularly exciting open question for future work is determining what types of losses, regularization, and feature distributions can lead to a small γ such that the resulting model is sufficiently private.

2.2 Comparison against neural network experiments

Although neural networks models are much more complex than logistic regression, we consider the following setting in which we can theoretically demonstrate the same phenomena we observe empirically for neural networks. For a realistic comparison, we require a setting in which benign overfitting occurs. To that end we define a bi-level feature ensemble similar to that considered in [15, 16]. In this model, we define Σ and β^* for some $d < p$ and $\eta > 0$ as

$$[\Sigma]_{k,k'}^2 = \begin{cases} \frac{p}{d} & \text{if } 1 \leq k = k' \leq d, \\ \frac{\eta p}{p-d} & \text{if } d < k = k' \leq p, \\ 0 & \text{if } k \neq k' \end{cases}, \quad \beta_k^* \sim \begin{cases} \mathcal{N}(0, \sigma_\beta^2) & \text{if } 1 \leq k \leq d, \\ 0 & \text{if } d < k \leq p \end{cases} \quad (4)$$

In this way, there is always a total variance of 1 in the first d features and of η in the tail of $p - d$ features. As $\phi = p/d \rightarrow \infty$, this model is known to exhibit benign overfitting [16].

Our logistic regression model does not admit a notion of training epochs, but because of the strong connection between ridge regularization and early stopping [42, 43], we use a decrease of regularization strength as a theoretical proxy for more training epochs.

To generate theoretical plots in the subsequent sections for specific settings, we solve the nonlinear system from Theorem 3 in Appendix B.2 due to [40] to characterize generalization error. Then using Theorem 1 and numerical integration we compute $\text{Adv}(A^*)$ for the optimal sample-specific loss thresholding adversary A^* as we describe in Appendix E. We also refer the reader to Appendix F for simulations that verify our computations of the sample-specific training and test densities.

3 Parameter-wise and epoch-wise privacy–utility trade-offs

We now demonstrate that there are privacy–utility trade-offs as a function of either the number of model parameters or training epochs individually. Specifically, when increasing the number either of parameters or training epochs, the resulting machine learning model generally becomes more accurate (improved generalization performance) but becomes less private (higher MI advantage of the adversary). The increase in accuracy has been discussed in detail in the double descent literature, and we refer readers to [6, 5, 17]. The decrease of privacy with overparameterization on MI has been observed for linear regression models in [22], but we show here that the phenomenon is robust, extending to classification models and even highly nonlinear models such as deep neural networks. We show the increase in the adversary’s MI advantage with parameters and epochs experimentally on various machine learning tasks and provide theoretical insights to their origins. All experimental details not included in the main text can be found in Appendix G. In all neural network plots, shaded areas indicate one standard deviation over repeated trials.

3.1 Parameter-wise privacy–utility trade-off: Empirical demonstration

We begin our demonstration on SVMs and plot both an adversary’s membership advantage and the SVM model’s validation error as a function of the number of parameters in Figure 2. We observe how MI increases (thus damaging privacy) while test error decreases (yielding a more accurate model) as the number of parameters grows. We consider data models based on those that have been shown to exhibit double descent in the overparameterized machine learning literature, including the weak features ensemble from [15], separable Gaussians with irrelevant features (based on synthetic dataset 1 of [44]), random ReLU features [45], and

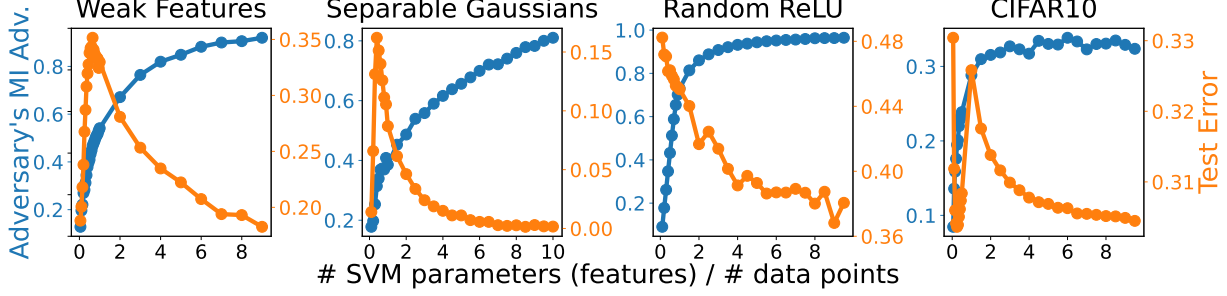


Figure 2: **Privacy vs. parameters (SVMs).** We demonstrate on SVMs for a variety of feature models how increasing overparameterization increases the adversary’s MI advantage on the SVM model even as it decreases validation error. Thus, number of parameters induces a privacy–utility trade-off.

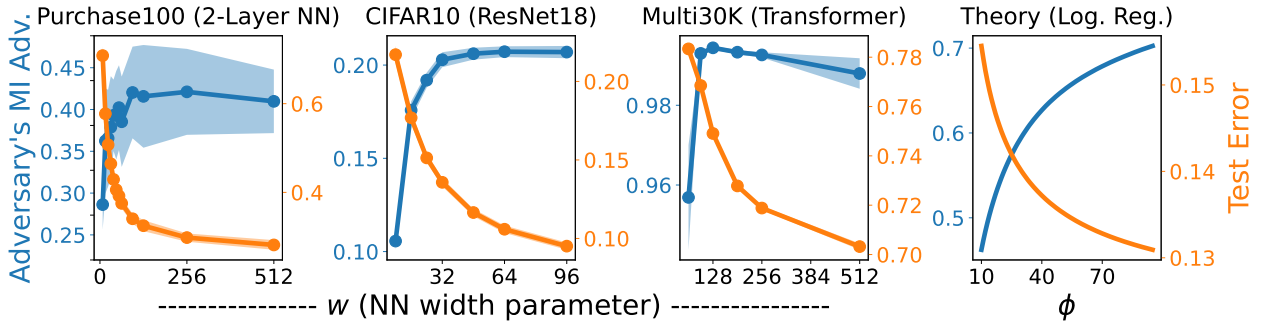


Figure 3: **Privacy vs. parameters (NNs and theory).** For NNs trained to optimal early stopping with respect to validation error, increasing the network’s width generally increases MI advantage on the network even as it decreases its test error. We see a similar effect for logistic regression with the bi-level ensemble theoretically when λ is tuned to minimize test error.

random projections on CIFAR10. For the MI attack, we estimate the optimal adversary attack of [22] by approximating the model output distributions as discrete histograms using Monte Carlo sampling over a minimum of 20,000 trials.

In Figure 3, we demonstrate that the same phenomenon occurs in NNs. Specifically, we consider NNs that are trained with optimal (with respect to validation error) early stopping: we stop training at the number of training epochs that maximizes validation accuracy. We consider three machine learning tasks: feature vector classification on the Purchase100 dataset [13] using a 2-layer NN, image classification on CIFAR10 [46] using the ResNet18 architecture [47], and language translation on the Multi30K dataset [48] using the Transformer architecture [49]. We control the number of parameters of the networks by scaling the size of the hidden dimensions by a width parameter w . For the MI attack, we use the sample-specific loss threshold attack, where the loss threshold is learned over reference models. This attack is introduced and detailed as “Attack R” in [41].

3.2 Parameter-wise trade-off: Theoretical insights

Using our theoretical tool from Theorem 1, we can in fact prove that for an extremely broad class of settings, including the bi-level ensemble which exhibits benign overfitting, overparameterization leads to perfect MI by nearly any adversary. We have omitted some technical conditions related to the convergence of a system of fixed point equations for the statement of part (a); please see Theorem 5 in Appendix D for precise details. In these statements, we assume all scalar variables (such as λ and η) to be fixed unless otherwise specified.

Theorem 2. *If $\hat{f}(\mathbf{x}) = \mathbf{x}^\top \hat{\beta}$ for $\hat{\beta}$ the solution to (2) and for some $\tau > 0$ we have an adversary $A(f, \mathbf{x}, y) = \mathbb{1}\{\ell(y, f(\mathbf{x})) < \tau\}$, then as $n, p \rightarrow \infty$ with $n/p \rightarrow \delta \in (0, \infty)$,*

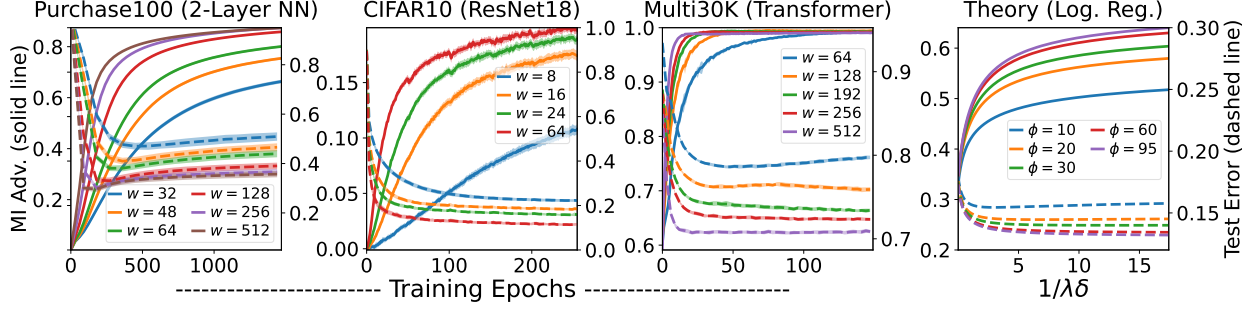


Figure 4: **Privacy vs. epochs.** Regardless of neural network width (parameterized by w), increasing the number of training epochs increases the adversary’s MI advantage (solid line) while simultaneously decreasing its test error (dashed line). This induces an epoch-wise privacy–utility trade-off. We demonstrate this phenomenon for various machine learning tasks and architectures: classification on Purchase100 with a 2-layer network, image classification on CIFAR10 with ResNet18, and language translation on Multi30K with Transformers.

- (a) If $\lim_{p \rightarrow \infty} \|\Sigma^{1/2}\beta^*\|_2/\sqrt{p}$ exists and is finite, and $\liminf_{p \rightarrow \infty} \lambda_{\min}(\Sigma) > 0$, where $\lambda_{\min}(\Sigma)$ is the smallest eigenvalue of Σ , then as $\delta \rightarrow 0$, $\text{Adv}(A) \rightarrow 1$.
- (b) For the bi-level ensemble in (4), if $p/d \rightarrow \phi \in (1, \infty)$ and d/n converges to a fixed value, then as $\phi \rightarrow \infty$, $\text{Adv}(A) \rightarrow 1$, and in the limit as $\lambda \rightarrow \infty$, $\mathcal{E}(f)$ is decreasing in ϕ .

This theorem highlights that as $\delta \rightarrow 0$, which means that the model becomes increasingly overparameterized, *any* constant-threshold adversary’s MI advantage converges to 1, and the adversary can perform perfect MI attacks on the learned model. We emphasize that the constant-threshold adversary is much weaker than the sample-specific loss threshold adversary we consider in our experiments, yet overparameterized models are still vulnerable. This is true regardless of any (fixed) value of regularization strength, meaning that ridge regularization is not sufficient to protect against MI attacks, echoing what was observed by [22] in linear regression. This result applies not only to standard isotropic data covariances, but also to highly anisotropic covariances such as the bi-level ensemble.

Part (b) highlights how in the right circumstances, we can still see generalization performance improving with overparameterization—that there is a trade-off between generalization and privacy, just as in our experimental results. We illustrate this alongside neural networks in Figure 3 for the bi-level model with fixed $n/d = 5$, $\sigma_\beta = 10$, and $\eta = 1$, with λ tuned to minimize test error, analogously to the optimal validation error early stopping in the NN experiments. We see that the generalization error decreases but the adversary’s MI advantage increases as the length of the tail of small eigenvalues of Σ increases for larger values of ϕ .

3.3 Epoch-wise privacy–utility trade-off

Using the same classification tasks and NN architectures as in Section 3.1, we empirically demonstrate the epoch-wise privacy–utility trade-off in Figure 4, where we plot the adversary’s MI advantage and the model’s generalization error as a function of training epochs. We also show that this phenomenon happens for a variety of NN widths. Similarly, using the same bi-level ensemble setup as in Section 3.2, we plot the adversary’s MI advantage and the model’s generalization error as a function of regularization strength (specifically plotting as a function of $1/\lambda\delta$ to more closely match the NN experiments) for a variety of values of ϕ .

An interesting observation from Figure 4 is that the adversary’s MI advantage can continue to increase even if test error stays the same. Thus, generalization error does not completely characterize membership inference. Instead, what leads to the increase in MI advantage is the increasing generalization (cross-entropy) loss gap. As the network is trained for more epochs, its training loss decreases at a greater rate than its test loss. Thus, it becomes easier to divide the training and test losses with a loss threshold, as illustrated in Figure 1, and continues to do so even after test error has converged.

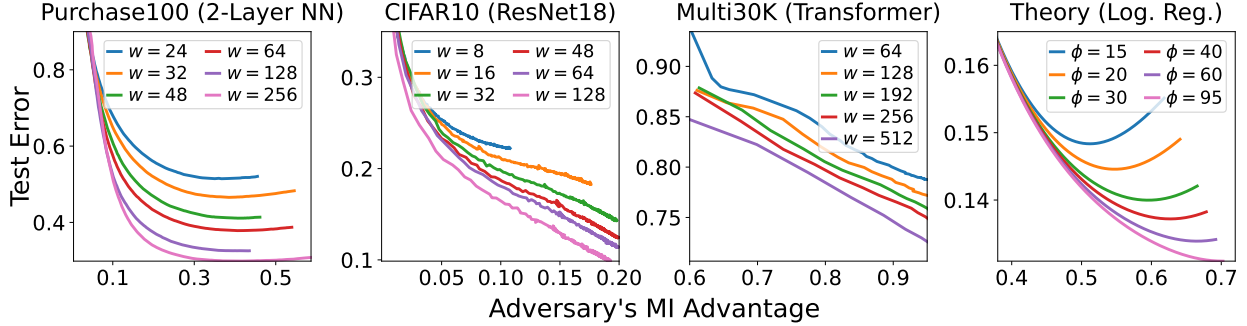


Figure 5: **Trade-offs are better with increased width.** We plot the epoch-wise privacy–utility trade-off of networks of different widths by sweeping through different training epochs. Observe that, for sufficiently low validation errors, wider networks are closer to the lower-left (high accuracy, high privacy) region compared to narrower networks.

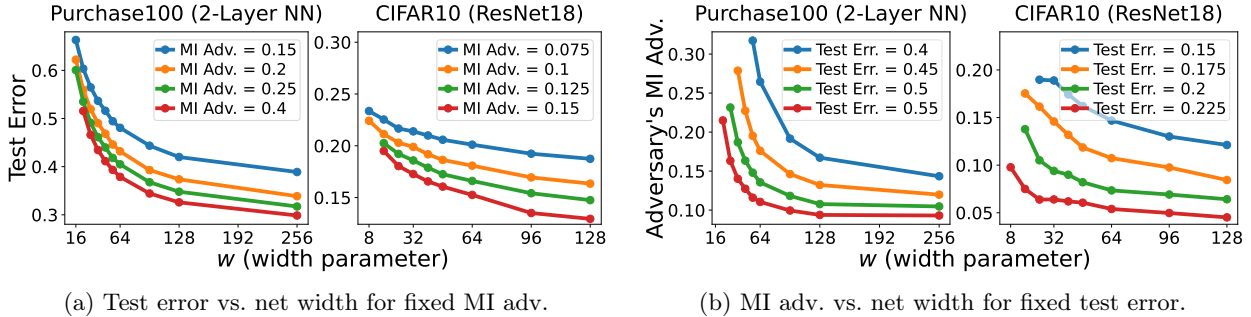


Figure 6: **Overparameterization with early stopping eliminates the privacy–utility trade-off.** (a) For each network width, we train the network until it reaches a given MI advantage value. We then plot the test error of the networks. Observe how test error decreases with parameters at a fixed MI advantage value. Thus, this eliminates the privacy–utility trade-off. Proper tuning of parameters and epochs together improves model accuracy without damaging its privacy. (b) Same as (a) but switching the roles of MI advantage and test error.

4 Benign overparameterization: Eliminating the privacy–utility trade-off

We now show that, perhaps counter-intuitively, if we jointly tune both the numbers of parameters and training epochs, we can eliminate the privacy–utility trade-off. The main idea is to *increase* the number of parameters while *decreasing* the number of training epochs at an appropriate rate.

4.1 Empirical observations: Better trade-offs with overparameterization

Our key observation is that the decrease in the model’s generalization error and the increase in an adversary’s MI advantage occur at different rates for models of different widths (recall Figure 4). However, it is difficult to draw conclusions about how the privacy–utility trade-off might vary with NN width from plots as a function of training epochs. Hence, we plot parametric curves for varying widths as a function of training epochs in a *privacy–utility plane* in Figure 5, which enables us to abstract away the number of epochs and compare trade-off curves across widths directly. In the plot, ideal performance is the lower-left corner, as this represents low MI advantage (high privacy) and low test error. In this representation, the story becomes clear: wider networks induce better privacy–utility trade-offs. That is, they are both below and to the left of the trade-off curves for narrower networks. The same occurs for logistic regression with the bi-level ensemble.

4.2 Eliminating the privacy–utility trade-off in practice: Privacy-based early stopping

We explicitly show how early stopping (with the appropriate stopping rule) *eliminates* the privacy–utility trade-off for overparameterization in Figure 6.¹ If we tune the number of training epochs for each width such that a fixed MI advantage is reached (which takes fewer epochs for larger widths), then we see from Figure 6a that overparameterization only *decreases* the generalization error. Similarly, tuning the number of epochs to a fixed validation error results in a decrease of the adversary’s MI advantage with increasing width, as shown in Figure 6b.

The takeaway for machine learning system designers is clear: **With proper early stopping of training, overparameterization only improves generalization performance without harming privacy.** Practitioners should opt for a wider network when available and use early stopping to achieve the required privacy budget. This thinking admits the simple implementation in Algorithm 1.

Algorithm 1: Privacy-based early stopping for model training

Data: training set $\mathcal{S}_{\text{train}} \sim \mathcal{D}^{n_{\text{train}}}$, validation set $\mathcal{S}_{\text{val}} \sim \mathcal{D}^{n_{\text{val}}}$, privacy estimation interval T , Adv_{max}

```

 $\hat{f}_0 \leftarrow \text{init}();$ 
for  $t = 1, 2, \dots$  do
     $\hat{f}_t \leftarrow \text{train}(\hat{f}_{t-1});$ 
    if  $t \equiv 0 \pmod{T}$  then
         $\widehat{\text{Adv}} \leftarrow \max_{\tau} \frac{|\{(\mathbf{x}, y) \in \mathcal{S}_{\text{train}} : \ell(y, \hat{f}_t(\mathbf{x})) < \tau\}|}{n_{\text{train}}} - \frac{|\{(\mathbf{x}, y) \in \mathcal{S}_{\text{val}} : \ell(y, \hat{f}_t(\mathbf{x})) < \tau\}|}{n_{\text{val}}};$ 
        if  $\widehat{\text{Adv}} > \text{Adv}_{\text{max}}$  then
            return  $\hat{f}_{t-T};$ 
```

The procedure is simple: Train as normal on the training set $\mathcal{S}_{\text{train}}$, and every T training epochs, use both the training set and the holdout set \mathcal{S}_{val} to estimate $\widehat{\text{Adv}}$, the constant loss thresholding adversary’s MI advantage, via the formula (5). This expression can be computed efficiently in time linear in the number of samples. Once this estimate $\widehat{\text{Adv}}$ exceeds some privacy budget Adv_{max} , revert back to the last sufficiently private model \hat{f}_{t-T} .

5 Discussion

On the empirical side, as we have made clear in this paper, the fact that the privacy–utility trade-off can be eliminated for overparameterization by simply early stopping is a boon for practitioners who wish to take advantage of the observed benefits of overparameterized models while preserving the privacy of their training data. It is an interesting open question whether the trade-off is also eliminated for combinations of overparameterization and other privacy-preserving mechanisms aside from early stopping. We are aware of one similar observation from recent work, where [35] observe a similar effect for differentially private fine-tuning of language models.

On the theoretical side, our observation that overparameterized models have better privacy–utility trade-offs has important takeaways for future study. Highly overparameterized models not only have more capacity to memorize than smaller networks, but they also appear to learn the underlying structure of the data much more quickly. In particular, wider networks appear to learn the training data’s structure more quickly than they memorize the actual training data points, such that, for a given level of privacy, they have better generalization performance than narrower networks. Identifying the mechanism that provides this benefit in overparameterized models and developing appropriate measures for an “effective” number of parameters that reflects the memorization capacity of the model as a function of both the true number of parameters and forms of regularization are important open questions. We believe our new leave-one-out characterization of the training output distribution in Theorem 1 will be helpful in answering these questions with respect to privacy.

¹The same trend holds for Transformers on Multi30K. We defer this plot to the Appendix.

6 Acknowledgments

This work was supported by NSF grants CCF-1911094, IIS-1838177, and IIS-1730574; ONR grants N00014-18-12571, N00014-20-1-2534, and MURI N00014-20-1-2787; AFOSR grant FA9550-22-1-0060; and a Vannevar Bush Faculty Fellowship, ONR grant N00014-18-1-2047.

References

- [1] Nelson Morgan and Hervé Bourlard. Generalization and parameter estimation in feedforward nets: Some experiments. *Advances in neural information processing systems*, 2, 1989.
- [2] Lutz Prechelt. Early stopping-but when? In *Neural Networks: Tricks of the trade*, pages 55–69. Springer, 1998.
- [3] Yann LeCun, John Denker, and Sara Solla. Optimal brain damage. *Advances in neural information processing systems*, 2, 1989.
- [4] V. N. Vapnik and A. Ya. Chervonenkis. On the uniform convergence of relative frequencies of events to their probabilities. *Theory of Probability & Its Applications*, 16(2):264–280, 1971. doi: 10.1137/1116025. URL <https://doi.org/10.1137/1116025>.
- [5] Preetum Nakkiran, Gal Kaplun, Yamini Bansal, Tristan Yang, Boaz Barak, and Ilya Sutskever. Deep double descent: Where bigger models and more data hurt. *Journal of Statistical Mechanics: Theory and Experiment*, 2021(12):124003, 2021.
- [6] Mikhail Belkin, Daniel Hsu, Siyuan Ma, and Soumik Mandal. Reconciling modern machine-learning practice and the classical bias–variance trade-off. *Proceedings of the National Academy of Sciences*, 116(32):15849–15854, 2019.
- [7] Peter L Bartlett, Philip M Long, Gábor Lugosi, and Alexander Tsigler. Benign overfitting in linear regression. *Proceedings of the National Academy of Sciences*, 117(48):30063–30070, 2020.
- [8] Mia Xu Chen, Benjamin N Lee, Gagan Bansal, Yuan Cao, Shuyuan Zhang, Justin Lu, Jackie Tsay, Yinan Wang, Andrew M Dai, Zhifeng Chen, et al. Gmail smart compose: Real-time assisted writing. In *Proceedings of the 25th ACM SIGKDD International Conference on Knowledge Discovery & Data Mining*, pages 2287–2295, 2019.
- [9] Google. Learn how google improves speech models. URL <https://support.google.com/assistant/answer/11140942?hl=en>.
- [10] Zeynep Batmaz, Ali Yurekli, Alper Bilge, and Cihan Kaleli. A review on deep learning for recommender systems: challenges and remedies. *Artificial Intelligence Review*, 52(1):1–37, 2019.
- [11] Nicholas Carlini, Florian Tramer, Eric Wallace, Matthew Jagielski, Ariel Herbert-Voss, Katherine Lee, Adam Roberts, Tom Brown, Dawn Song, Ulfar Erlingsson, et al. Extracting training data from large language models. In *30th USENIX Security Symposium (USENIX Security 21)*, pages 2633–2650, 2021.
- [12] Matt Fredrikson, Somesh Jha, and Thomas Ristenpart. Model inversion attacks that exploit confidence information and basic countermeasures. In *Proceedings of the 22nd ACM SIGSAC conference on computer and communications security*, pages 1322–1333, 2015.
- [13] Reza Shokri, Marco Stronati, Congzheng Song, and Vitaly Shmatikov. Membership inference attacks against machine learning models. In *2017 IEEE Symposium on Security and Privacy (SP)*, pages 3–18. IEEE, 2017.
- [14] Nicholas Carlini, Steve Chien, Milad Nasr, Shuang Song, Andreas Terzis, and Florian Tramer. Membership inference attacks from first principles. *arXiv preprint arXiv:2112.03570*, 2021.

- [15] Vidya Muthukumar, Adhyayan Narang, Vignesh Subramanian, Mikhail Belkin, Daniel Hsu, and Anant Sahai. Classification vs regression in overparameterized regimes: Does the loss function matter? *Journal of Machine Learning Research*, 22(222):1–69, 2021.
- [16] Ke Wang and Christos Thrampoulidis. Benign overfitting in binary classification of gaussian mixtures. In *ICASSP 2021-2021 IEEE International Conference on Acoustics, Speech and Signal Processing (ICASSP)*, pages 4030–4034. IEEE, 2021.
- [17] Yehuda Dar, Vidya Muthukumar, and Richard G Baraniuk. A farewell to the bias-variance tradeoff? an overview of the theory of overparameterized machine learning. *arXiv preprint arXiv:2109.02355*, 2021.
- [18] Hongsheng Hu, Zoran Salcic, Gillian Dobbie, and Xuyun Zhang. Membership inference attacks on machine learning: A survey. *arXiv preprint arXiv:2103.07853*, 2021.
- [19] Alexandre Sablayrolles, Matthijs Douze, Cordelia Schmid, Yann Ollivier, and Hervé Jégou. White-box vs black-box: Bayes optimal strategies for membership inference. In *International Conference on Machine Learning*, pages 5558–5567. PMLR, 2019.
- [20] Yunhui Long, Vincent Bindschaedler, and Carl A Gunter. Towards measuring membership privacy. *arXiv preprint arXiv:1712.09136*, 2017.
- [21] Ahmed Salem, Yang Zhang, Mathias Humbert, Pascal Berrang, Mario Fritz, and Michael Backes. ML-leaks: Model and data independent membership inference attacks and defenses on machine learning models. *arXiv preprint arXiv:1806.01246*, 2018.
- [22] Jasper Tan, Blake Mason, Hamid Javadi, and Richard G Baraniuk. Parameters or privacy: A provable tradeoff between overparameterization and membership inference. *arXiv preprint arXiv:2202.01243*, 2022.
- [23] Yigitcan Kaya and Tudor Dumitras. When does data augmentation help with membership inference attacks? In *International Conference on Machine Learning*, pages 5345–5355. PMLR, 2021.
- [24] Erick Galinkin. The influence of dropout on membership inference in differentially private models. *arXiv preprint arXiv:2103.09008*, 2021.
- [25] Yijue Wang, Chenghong Wang, Zigeng Wang, Shanglin Zhou, Hang Liu, Jinbo Bi, Caiwen Ding, and Sanguthevar Rajasekaran. Against membership inference attack: Pruning is all you need. *arXiv preprint arXiv:2008.13578*, 2020.
- [26] Liwei Song, Reza Shokri, and Prateek Mittal. Membership inference attacks against adversarially robust deep learning models. In *2019 IEEE Security and Privacy Workshops (SPW)*, pages 50–56. IEEE, 2019.
- [27] Shahbaz Rezaei, Zubair Shafiq, and Xin Liu. Accuracy-privacy trade-off in deep ensemble. *arXiv preprint arXiv:2105.05381*, 2021.
- [28] Cynthia Dwork. Differential privacy: A survey of results. In *International conference on theory and applications of models of computation*, pages 1–19. Springer, 2008.
- [29] Trung Ha, Tran Khanh Dang, Tran Tri Dang, Tuan Anh Truong, and Manh Tuan Nguyen. Differential privacy in deep learning: an overview. In *2019 International Conference on Advanced Computing and Applications (ACOMP)*, pages 97–102. IEEE, 2019.
- [30] Samuel Yeom, Irene Giacomelli, Matt Fredrikson, and Somesh Jha. Privacy risk in machine learning: Analyzing the connection to overfitting. In *2018 IEEE 31st Comput. Security Found. Symp. (CSF)*, pages 268–282, 2018. doi: 10.1109/CSF.2018.00027.
- [31] Martin Abadi, Andy Chu, Ian Goodfellow, H Brendan McMahan, Ilya Mironov, Kunal Talwar, and Li Zhang. Deep learning with differential privacy. In *Proceedings of the 2016 ACM SIGSAC conference on computer and communications security*, pages 308–318, 2016.

- [32] Lei Yu, Ling Liu, Calton Pu, Mehmet Emre Gursoy, and Stacey Truex. Differentially private model publishing for deep learning. In *2019 IEEE Symposium on Security and Privacy (SP)*, pages 332–349. IEEE, 2019.
- [33] Mark Bun, Jonathan Ullman, and Salil Vadhan. Fingerprinting codes and the price of approximate differential privacy. *SIAM Journal on Computing*, 47(5):1888–1938, 2018.
- [34] Xiaoyong Yuan and Lan Zhang. Membership inference attacks and defenses in neural network pruning. *arXiv preprint arXiv:2202.03335*, 2022.
- [35] Da Yu, Saurabh Naik, Arturs Backurs, Sivakanth Gopi, Huseyin A Inan, Gautam Kamath, Janardhan Kulkarni, Yin Tat Lee, Andre Manoel, Lukas Wutschitz, et al. Differentially private fine-tuning of language models. *arXiv preprint arXiv:2110.06500*, 2021.
- [36] Christos Thrampoulidis, Ehsan Abbasi, and Babak Hassibi. Precise error analysis of regularized m -estimators in high dimensions. *IEEE Transactions on Information Theory*, 64(8):5592–5628, 2018. doi: 10.1109/TIT.2018.2840720.
- [37] Melikasadat Emami, Mojtaba Sahraee-Ardakan, Parthe Pandit, Sundeep Rangan, and Alyson Fletcher. Generalization error of generalized linear models in high dimensions. In Hal Daumé III and Aarti Singh, editors, *Proceedings of the 37th International Conference on Machine Learning*, volume 119 of *Proceedings of Machine Learning Research*, pages 2892–2901. PMLR, 13–18 Jul 2020. URL <https://proceedings.mlr.press/v119/emami20a.html>.
- [38] Cedric Gerbelot, Alia Abbara, and Florent Krzakala. Asymptotic errors for teacher-student convex generalized linear models (or: How to prove kabashima’s replica formula). *arXiv preprint arXiv:2006.06581*, 2020.
- [39] Alyson K Fletcher, Sundeep Rangan, and Philip Schniter. Inference in deep networks in high dimensions. In *2018 IEEE International Symposium on Information Theory (ISIT)*, pages 1884–1888. IEEE, 2018.
- [40] Fariborz Salehi, Ehsan Abbasi, and Babak Hassibi. The impact of regularization on high-dimensional logistic regression. In *Advances in Neural Information Processing Systems*, volume 32, 2019.
- [41] Jiayuan Ye, Aadyaa Maddi, Sasi Kumar Murakonda, and Reza Shokri. Enhanced membership inference attacks against machine learning models. *arXiv preprint arXiv:2111.09679*, 2021.
- [42] Arun Suggala, Adarsh Prasad, and Pradeep K Ravikumar. Connecting optimization and regularization paths. In *Advances in Neural Information Processing Systems*, volume 31, 2018.
- [43] Alnur Ali, J. Zico Kolter, and Ryan J. Tibshirani. A continuous-time view of early stopping for least squares regression. In *Proceedings of the Twenty-Second International Conference on Artificial Intelligence and Statistics*, volume 89 of *Proceedings of Machine Learning Research*, pages 1370–1378. PMLR, 16–18 Apr 2019.
- [44] Mikhail Belkin, Siyuan Ma, and Soumik Mandal. To understand deep learning we need to understand kernel learning. In *International Conference on Machine Learning*, pages 541–549. PMLR, 2018.
- [45] Andrea Montanari, Feng Ruan, Youngtak Sohn, and Jun Yan. The generalization error of max-margin linear classifiers: High-dimensional asymptotics in the overparametrized regime. *arXiv preprint arXiv:1911.01544*, 2019.
- [46] Alex Krizhevsky, Geoffrey Hinton, et al. Learning multiple layers of features from tiny images. 2009.
- [47] Kaiming He, Xiangyu Zhang, Shaoqing Ren, and Jian Sun. Deep residual learning for image recognition. In *Proceedings of the IEEE conference on computer vision and pattern recognition*, pages 770–778, 2016.
- [48] Desmond Elliott, Stella Frank, Khalil Sima’an, and Lucia Specia. Multi30k: Multilingual english-german image descriptions. *arXiv preprint arXiv:1605.00459*, 2016.

- [49] Ashish Vaswani, Noam Shazeer, Niki Parmar, Jakob Uszkoreit, Llion Jones, Aidan N Gomez, Łukasz Kaiser, and Illia Polosukhin. Attention is all you need. *Advances in neural information processing systems*, 30, 2017.
- [50] Fabian Pedregosa, Gaël Varoquaux, Alexandre Gramfort, Vincent Michel, Bertrand Thirion, Olivier Grisel, Mathieu Blondel, Peter Prettenhofer, Ron Weiss, Vincent Dubourg, et al. Scikit-learn: Machine learning in python. *the Journal of machine Learning research*, 12:2825–2830, 2011.
- [51] Daniel Soudry, Elad Hoffer, Mor Shpigel Nacson, Suriya Gunasekar, and Nathan Srebro. The implicit bias of gradient descent on separable data. *The Journal of Machine Learning Research*, 19(1):2822–2878, 2018.
- [52] Ziwei Ji and Matus Telgarsky. The implicit bias of gradient descent on nonseparable data. In *Conference on Learning Theory*, pages 1772–1798. PMLR, 2019.
- [53] Ali Rahimi, Benjamin Recht, et al. Random features for large-scale kernel machines. In *NIPS*, volume 3, page 5. Citeseer, 2007.
- [54] Diederik P Kingma and Jimmy Ba. Adam: A method for stochastic optimization. *arXiv preprint arXiv:1412.6980*, 2014.

A Limitations and Broader Impacts

A.1 Limitations of this work

A possible limitation of this work is that we focus on a particular class of inference attacks, the loss threshold attack, in most of our experimental results, though we note that as [19] and [22] both argue, the loss threshold attack is essentially optimal for membership inference for many data distributions. More subtly, the procedure we propose for estimating membership inference vulnerability involves computing an empirical estimate. As such, there is uncertainty in this process. In practical settings where the training and validation sets are large, this is likely not a major concern. That said, in settings where the privacy budget is very low and/or privacy is paramount it may additionally be necessary to use high-probability bounds on the adversary’s MI advantage rather than the estimate directly for an added layer of security. Furthermore, the theoretical guarantees are in the asymptotic regime. While they show a strong correlation with finite dimension experiments (e.g., Figure 4), developing tight, non-asymptotic results is an open question. [16], for instance, is able to derive non-asymptotic guarantees to connect generalization error to overparameterization, but the same technique does not apply in the case of membership inference: it is important to consider the distribution of the model’s output for specific inputs—not just the population on average.

A.2 Ethical Considerations

Ensuring that models protect the data that they are trained on is important for modern machine learning systems. In order to achieve benign overparameterization for membership inference and generalization error jointly, we perform precise tuning and early stopping. When implementing these ideas in practical scenarios, it is recommended that a sensitivity analysis additionally be conducted to ensure that the chosen parameters are sufficiently tight. Without doing so, applying this method may lead to false confidence in a method’s robustness to MI attacks. In general, the authors believe that in settings where privacy is of the utmost concern, such as when training with medical data, additional measures beyond those covered in this work should be taken to ensure that the data stays private. Finally, this paper focuses on membership inference in particular and these results are not as general as complete differential privacy. Practitioners should consider additional privacy vulnerabilities beyond membership inference alone.

B Background material

Here we include a few definitions and results borrowed from other works.

B.1 Definitions

We define the proximal operator for a function Ω as follows.

Definition 2 (Proximal operator). *The proximal operator of a function $\Omega: \mathbb{R}^p \rightarrow \mathbb{R}$ is defined as*

$$\text{Prox}_{\Omega}(\mathbf{v}) = \arg \min_{\mathbf{w} \in \mathbb{R}^p} \Omega(\mathbf{w}) + \frac{1}{2} \|\mathbf{w} - \mathbf{v}\|_2. \quad (6)$$

It will be valuable to consider the first-order optimality condition of the proximal operator; for differentiable penalties, the minimizer \mathbf{w}^* satisfies

$$\nabla \Omega(\mathbf{w}^*) + \mathbf{w} - \mathbf{v} = \mathbf{0}. \quad (7)$$

For our work, we will need the form of the scalar proximal operator for $\Omega(\mathbf{v}) = \frac{1}{2} \|\mathbf{A}\mathbf{v}\|_2^2$ for symmetric $\mathbf{A} \in \mathbb{R}^{p \times p}$, which for $t > 0$ is given by

$$\text{Prox}_{t\Omega}(\mathbf{v}) = (\mathbf{I}_p + t\mathbf{A}^2)^{-1} \mathbf{v}. \quad (8)$$

We also have the definition of local Lipschitzness from Salehi et al. [40].

Definition 3 (Locally Lipschitz). *A function $\Phi: \mathbb{R}^d \rightarrow \mathbb{R}$ is said to be locally Lipschitz if $\forall M > 0, \exists L_M \geq 0$, such that $\forall \mathbf{x}, \mathbf{y} \in [-M, +M]^d, |\Phi(\mathbf{x}) - \Phi(\mathbf{y})| \leq L_M \|\mathbf{x} - \mathbf{y}\|$.*

B.2 Fixed point equations for logistic regression

We borrow the following theorem (slightly adapted to our notation) from Salehi et al. [40].

Theorem 3 (Theorem 1 of Salehi et al. [40]). *For training data $\mathbf{x}_i \stackrel{\text{i.i.d.}}{\sim} \mathcal{N}(\mathbf{0}, \frac{1}{p}\mathbf{I}_p)$ and $y_i \sim \text{Bernoulli}(\mathbf{x}_i^\top \boldsymbol{\beta}^*)$, consider the optimization program*

$$\hat{\boldsymbol{\beta}} = \arg \min_{\boldsymbol{\beta} \in \mathbb{R}^p} \frac{1}{n} \sum_{i=1}^n \ell(y_i, \mathbf{x}_i^\top \boldsymbol{\beta}) + \frac{\lambda}{p} \Omega(\boldsymbol{\beta}), \quad (9)$$

where $\ell(y, z) = \rho(z) - yz$ for $\rho(z) = \log(1 + \exp(-z))$ is the logistic loss, and $\Omega: \mathbb{R}^p \rightarrow \mathbb{R}$ is a convex regularization function. Consider also the following nonlinear system

$$\left\{ \begin{array}{l} \kappa^2 \alpha = \frac{1}{p} \boldsymbol{\beta}^{*\top} \text{Prox}_{\lambda \sigma \tau \Omega} \left(\sigma \tau (\theta \boldsymbol{\beta}^* + \frac{r}{\sqrt{\delta}} \mathbf{g}) \right), \\ \gamma = \frac{1}{r \sqrt{\delta} p} \mathbf{g}^\top \text{Prox}_{\lambda \sigma \tau \Omega} \left(\sigma \tau (\theta \boldsymbol{\beta}^* + \frac{r}{\sqrt{\delta}} \mathbf{g}) \right), \\ \kappa^2 \alpha^2 + \sigma^2 = \frac{1}{p} \left\| \text{Prox}_{\lambda \sigma \tau \Omega} \left(\sigma \tau (\theta \boldsymbol{\beta}^* + \frac{r}{\sqrt{\delta}} \mathbf{g}) \right) \right\|_2^2, \\ \gamma^2 = \frac{2}{r^2} \mathbb{E} \left[\rho'(-\kappa Z_1) (\kappa \alpha Z_1 + \sigma Z_2 - \text{Prox}_{\gamma \rho}(\kappa \alpha Z_1 + \sigma Z_2))^2 \right], \\ \theta \gamma = -2 \mathbb{E} \left[\rho''(-\kappa Z_1) \text{Prox}_{\gamma \rho}(\kappa \alpha Z_1 + \sigma Z_2) \right], \\ 1 - \frac{\gamma}{\sigma \tau} = \mathbb{E} \left[\frac{2 \rho'(-\kappa Z_1)}{1 + \gamma \rho''(\text{Prox}_{\gamma \rho}(\kappa \alpha Z_1 + \sigma Z_2))} \right], \end{array} \right. \quad (10)$$

where $\mathbf{g} \sim \mathcal{N}(\mathbf{0}, \mathbf{I}_p)$ is independent of $\boldsymbol{\beta}^*$ and Ω , and Z_1 and Z_2 are independent standard normal variables. Assume that as $p \rightarrow \infty$, $n/p \rightarrow \delta$, $\|\boldsymbol{\beta}\|_2/\sqrt{p} \rightarrow \kappa$, and that the system in (10) has a unique solution $(\bar{\alpha}, \bar{\sigma}, \bar{\gamma}, \bar{\theta}, \bar{\tau}, \bar{r})$. Then, as $p \rightarrow \infty$, for any locally-Lipschitz function $\Psi: \mathbb{R} \times \mathbb{R} \rightarrow \mathbb{R}$, we have

$$\frac{1}{p} \sum_{j=1}^p \Psi(\hat{\beta}_j, \beta_j^*) \xrightarrow{p} \frac{1}{p} \sum_{j=1}^p \Psi([\boldsymbol{\Gamma}(\boldsymbol{\beta}^*, \mathbf{g})]_j, \beta_j^*), \quad (11)$$

where $\boldsymbol{\Gamma}(\mathbf{v}, \mathbf{z}) = \text{Prox}_{\lambda \bar{\sigma} \bar{\tau} \Omega} \left(\bar{\sigma} \bar{\tau} (\bar{\theta} \mathbf{v} + \frac{\bar{r}}{\sqrt{\delta}} \mathbf{z}) \right)$.

The astute reader may note that Salehi et al. [40] require separable regularizers and drawing $\boldsymbol{\beta}^*$ element-wise i.i.d. from some distribution, but that neither of these are required for their proof technique to go through, so we have stated the more general result here, as we will need both of these assumptions to be relaxed.

C Leave-one-out analysis for membership inference

In order to study MI attacks, we need to understand how the distribution of training points differs from test points. We prove the following result to this end for logistic regression with a ridge penalty; however, the proof strategy is general and applies readily to other losses and penalties for general linear models that admit a result similar to Theorem 3, which includes many common models in machine learning [36–38].

Theorem 4. *Consider the solution $\hat{\boldsymbol{\beta}}$ to the optimization problem in (2). Let $\tilde{\boldsymbol{\beta}}^* = \boldsymbol{\Sigma}^{1/2} \boldsymbol{\beta}^*$, $\tilde{\mathbf{x}}_i = \boldsymbol{\Sigma}^{-1/2} \mathbf{x}_i$, and $\tilde{\Omega}(\tilde{\boldsymbol{\beta}}) = \frac{1}{2} \|\boldsymbol{\Sigma}^{-1/2} \tilde{\boldsymbol{\beta}}\|_2^2$. Assume Theorem 3 holds for $\tilde{\boldsymbol{\beta}}^*$ in place of $\boldsymbol{\beta}^*$ and $\tilde{\Omega}$ in place of Ω . Then for any training point \mathbf{x}_i ,*

$$\mathbf{x}_i^\top \hat{\boldsymbol{\beta}} \xrightarrow{d} \text{Prox}_{\tilde{\gamma} \ell(y_i, \cdot)} \left(\mathbf{x}_i^\top \hat{\boldsymbol{\beta}}_{-i} \right), \quad (12)$$

where $\bar{\gamma}$ is from the result of Theorem 3, and

$$\hat{\beta}_{-i} = \arg \min_{\beta \in \mathbb{R}^p} \frac{1}{n} \sum_{i' \neq i}^n \ell(y_{i'}, \mathbf{x}_{i'}^\top \beta) + \frac{\lambda}{2p} \|\beta\|_2^2. \quad (13)$$

Proof. We first make a leave-one-out modification the optimization problem for a general loss and regularizer:

$$\hat{\beta} = \Sigma^{-1/2} \cdot \arg \min_{\tilde{\beta}} \frac{1}{n} \sum_{i' \neq i}^n \ell(y_{i'}, \tilde{\mathbf{x}}_{i'}^\top \tilde{\beta}) + \frac{\lambda}{p} \bar{\Omega}(\tilde{\beta}), \quad (14)$$

where

$$\bar{\Omega}_i(\tilde{\beta}) = \tilde{\Omega}(\tilde{\beta}) + \frac{1}{\lambda \delta} \ell(y_i, \tilde{\mathbf{x}}_i^\top \tilde{\beta}). \quad (15)$$

Applying Theorem 3 to this problem, the solution is equivalent to one of the form

$$\hat{\beta}_{\text{equiv}} = \Sigma^{-1/2} \cdot \text{Prox}_{t\bar{\Omega}_i} \left(a\tilde{\beta}^* + b\mathbf{g} \right), \quad (16)$$

where $t = \lambda \bar{\sigma} \bar{\tau}$, $a = \bar{\sigma} \bar{\tau} \bar{\theta}$, and $b = \bar{\sigma} \bar{\tau} \bar{r} / \sqrt{\delta}$. This proximal operator is the solution \mathbf{w}^* to the equation

$$t \nabla \tilde{\Omega}(\mathbf{w}^*) + \frac{t}{\lambda \delta} \ell'(y_i, \tilde{\mathbf{x}}_i^\top \mathbf{w}^*) \tilde{\mathbf{x}}_i + \mathbf{w}^* - (a\tilde{\beta}^* + b\mathbf{g}) = 0, \quad (17)$$

where $\ell'(y_i, z) = \partial \ell(y_i, z) / \partial z$. Note that this is equivalent to

$$\mathbf{w}^* = \text{Prox}_{t\tilde{\Omega}} \left(a\tilde{\beta}^* + b\mathbf{g} - \frac{t}{\lambda \delta} \ell'(y_i, \tilde{\mathbf{x}}_i^\top \mathbf{w}^*) \tilde{\mathbf{x}}_i \right). \quad (18)$$

Here we specialize to the ridge penalty, but this can be extended to separable regularizers with careful application of Stein's lemma. Plugging in the form of the proximal operator for generalized ridge penalties, we have

$$\mathbf{w}^* = \Sigma (\Sigma + t\mathbf{I}_p)^{-1} \left(a\tilde{\beta}^* + b\mathbf{g} - \frac{t}{\lambda \delta} \ell'(y_i, \tilde{\mathbf{x}}_i^\top \mathbf{w}^*) \tilde{\mathbf{x}}_i \right). \quad (19)$$

We wish to characterize $\mathbf{x}_i^\top \hat{\beta}$, which is equivalent to characterizing $\mathbf{x}_i^\top \hat{\beta}_{\text{equiv}} = \tilde{\mathbf{x}}_i^\top \mathbf{w}^*$. Firstly, we note that for any random vector \mathbf{u} such that $\|\mathbf{u}\|_2^2 / \sqrt{p} \rightarrow C_{\mathbf{u}} < \infty$ that is independent of $\tilde{\mathbf{x}}_i$,

$$\frac{1}{p} \mathbf{u}^\top \mathbf{w}^* \xrightarrow{p} \frac{1}{p} \mathbf{u}^\top \Sigma (\Sigma + t\mathbf{I}_p)^{-1} (a\tilde{\beta}^* + b\mathbf{g}). \quad (20)$$

Appealing to Theorem 3 again, this means that the nonlinear system is in fact unaffected by our leave-one-out modification asymptotically, and that both cases have the same solution $(\bar{\alpha}, \bar{\sigma}, \bar{\gamma}, \bar{\theta}, \bar{\tau}, \bar{r})$ to the nonlinear system (10). Therefore,

$$\mathbf{x}_i^\top \hat{\beta}_{-i} \xrightarrow{d} \tilde{\mathbf{x}}_i^\top \Sigma (\Sigma + t\mathbf{I}_p)^{-1} (a\tilde{\beta}^* + b\mathbf{g}) \sim \mathcal{N}(0, \kappa^2 \bar{\alpha}^2 + \bar{\sigma}^2). \quad (21)$$

Since \mathbf{g} / \sqrt{p} and $\tilde{\mathbf{x}}_i$ have the same distribution, from the second equation in the nonlinear system (10) we know that

$$\tilde{\mathbf{x}}_i^\top \Sigma (\Sigma + t\mathbf{I}_p)^{-1} \tilde{\mathbf{x}}_i \xrightarrow{\text{a.s.}} \frac{1}{p} \mathbf{g}^\top \Sigma (\Sigma + t\mathbf{I}_p)^{-1} \mathbf{g} = \frac{\bar{\gamma} \delta}{\bar{\sigma} \bar{\tau}}. \quad (22)$$

All together, this gives us

$$\mathbf{x}_i^\top \hat{\beta} \xrightarrow{p} \tilde{\mathbf{x}}_i^\top \Sigma (\Sigma + t\mathbf{I}_p)^{-1} (a\tilde{\beta}^* + b\mathbf{g}) - \bar{\gamma} \ell'(y_i, \mathbf{x}_i^\top \hat{\beta}) \quad (23)$$

$$\implies \mathbf{x}_i^\top \hat{\beta} \xrightarrow{d} \text{Prox}_{\bar{\gamma} \ell(y_i, \mathbf{x}_i^\top \hat{\beta})} \left(\mathbf{x}_i^\top \hat{\beta}_{-i} \right), \quad (24)$$

which is the stated result. \square

D Formal version of Theorem 2 and proof

Theorem 2 is a slightly informal version of the following theorem. The only difference is technical, as we must assume the convergence of the nonlinear system (10) for part (a). The convergence of MI advantage to 1 of part (b) of Theorem 2 is implied by part (a) of the following theorem.

Theorem 5. *Consider the solution $\hat{\beta}$ to the optimization problem in (2). Then*

- (a) *If the result of Theorem 4 holds and the minimum eigenvalue of Σ is lower bounded by a positive constant for sufficiently small δ , then as $\delta \rightarrow 0$, $\text{Adv}(A) \rightarrow 1$.*
- (b) *For the bilevel model in (4), if $p/d \rightarrow \phi \in (1, \infty)$ and d/n converges to a fixed value, then in the limit as $\lambda \rightarrow \infty$, $\mathcal{E}(f)$ is decreasing in ϕ .*

This theorem makes claims of two natures: that MI advantage of the adversary goes to 1, and that generalization error is decreasing. For the former, we will show that the output distributions diverge for train and test points such that it becomes trivial to distinguish between the two distributions, and for the latter, we will determine the form of the generalization error and show that it is decreasing in the proposed variable.

D.1 Part (a): membership inference advantage

We will assume the notation and setting from the proof of Theorem 4. When rewriting equations from (10), we will omit the bars (e.g., $\bar{\gamma}$ in the next section) when describing general implications of the equations, and then use bars to describe conclusions about the *unique* fixed point solution that characterizes the limiting estimator, which we assumed to exist in applying Theorem 3.

D.1.1 Growth of $\bar{\gamma}$

First, we show that $\bar{\gamma}$, the scaling factor of the proximal operator in Theorem 4, tends to infinity as $\delta \rightarrow 0^+$. This will drive training points to be much different from test points as long as the test point distribution variance doesn't increase. From the sixth equation in the nonlinear system (10), since the right hand side is greater than 0 and the fixed point variables are non-negative, we can conclude that $\sigma\tau > \gamma$. We can combine this with the second equation to yield

$$\gamma = \frac{1}{p} \mathbf{g}^\top \Sigma (\Sigma + \lambda \sigma \tau \mathbf{I}_p)^{-1} \mathbf{g} \frac{\sigma \tau}{\delta} \quad (25)$$

$$= \frac{1}{\lambda \delta p} \mathbf{g}^\top \left(\frac{1}{\lambda \sigma \tau} \mathbf{I}_p + \Sigma^{-1} \right)^{-1} \mathbf{g} \quad (26)$$

$$> \frac{1}{\lambda \delta p} \mathbf{g}^\top \left(\frac{1}{\lambda \gamma} \mathbf{I}_p + \Sigma^{-1} \right)^{-1} \mathbf{g} \quad (27)$$

$$\xrightarrow{\text{a.s.}} \frac{1}{\lambda \delta p} \text{tr} \left[\left(\frac{1}{\lambda \gamma} \mathbf{I}_p + \Sigma^{-1} \right)^{-1} \right] \quad (28)$$

Because the smallest eigenvalue $\lambda_{\min}(\Sigma) > 0$, this implies that

$$\lambda \gamma > \frac{1}{\delta} \frac{1}{\frac{1}{\lambda \gamma} + \frac{1}{\lambda_{\min}(\Sigma)}} \implies \frac{\lambda \gamma}{\lambda_{\min}(\Sigma)} > \frac{1}{\delta} - 1. \quad (29)$$

Therefore, asymptotically, there exists a constant $c_{\bar{\gamma}} > 0$ such that for sufficiently small δ , we have $\lambda \bar{\gamma} \geq c_{\bar{\gamma}}/\delta$, so $\bar{\gamma} \rightarrow \infty$ as $\delta \rightarrow 0^+$.

D.1.2 Vanishing of output variance.

We next argue that $\kappa^2 \bar{\alpha}^2 + \bar{\sigma}^2$ tends to 0 as $\delta \rightarrow 0$. We remind the reader that as in the proof of Theorem 4, this is the variance of $\mathbf{x}_i^\top \hat{\beta}_{-i}$, which is also equal to the variance of the output for an unseen test point.

First, we consider the fourth equation in the nonlinear system (10). Applying the first-order optimality condition of the proximal operator, this is equivalent to

$$r^2 = 2 \mathbb{E} \left[\rho'(-\kappa Z_1) \rho'(\text{Prox}_{\gamma\rho}(\kappa\alpha Z_1 + \sigma Z_2))^2 \right] \leq 2. \quad (30)$$

Similarly, the fifth equation can be written as

$$\theta = \frac{-2}{\gamma} \mathbb{E} \left[\rho''(-\kappa Z_1) (\kappa\alpha Z_1 + \sigma Z_2 - \gamma \rho'(\text{Prox}_{\gamma\rho}(\kappa\alpha Z_1 + \sigma Z_2))) \right] \quad (31)$$

$$= 2 \mathbb{E} \left[\rho''(-\kappa Z_1) \rho'(\text{Prox}_{\gamma\rho}(\kappa\alpha Z_1 + \sigma Z_2)) \right] \quad (32)$$

$$\leq \frac{1}{2}, \quad (33)$$

where we have used the fact that the expectation of any odd function of a standard normal variable is zero, and that $\rho''(u) \leq 1/4$ for all $u \in \mathbb{R}$. Thus, both r and θ are upper bounded by constants. Let us now consider the third equation.

$$\kappa^2 \alpha^2 + \sigma^2 = \frac{(\sigma\tau)^2}{p} (\theta \tilde{\beta}^* + \frac{r}{\sqrt{\delta}} \mathbf{g})^\top \Sigma^2 (\Sigma + \lambda \sigma \tau \mathbf{I}_p)^{-2} (\theta \tilde{\beta}^* + \frac{r}{\sqrt{\delta}} \mathbf{g}) \quad (34)$$

$$\leq \frac{1}{\lambda^2} \left(\kappa^2 \theta^2 + \frac{r^2}{\delta} \right) \quad (35)$$

$$\leq \frac{1}{\lambda^2} \left(4\kappa^2 + \frac{1}{4\delta} \right). \quad (36)$$

Here the first inequality is obtained by letting $\sigma\tau$ tend to infinity, and the second is obtained by applying our upper bounds for θ and r . Therefore, for sufficiently small δ , there exists c_1 such that $\kappa^2 \alpha^2 + \sigma^2 \leq c_1^2 / \delta$.

We now wish to return to (30) and (32) to determine tighter upper bounds. To that end, we first prove the following lemma

Lemma 6. *Let Z be a standard normal random variable. For any $a_0, b_0 > 0$, there exist $\delta_0 > 0$ and $c > 0$ such that for all $a \geq a_0$, $b \leq b_0$, and $0 < \delta < \delta_0$,*

$$\Pr \left(\text{Prox}_{a\rho/\delta} \left(\frac{bZ}{\sqrt{\delta}} \right) > \log(c\delta \log(1/\delta)) \right) \leq \delta^2. \quad (37)$$

Proof. We begin by observing that is sufficient to prove the claim for $a = a_0$ and $b = b_0$, since the probability is monotonically decreasing and increasing, respectively, in each variable for sufficiently small δ . By standard Gaussian tail bounds, for sufficiently small δ ,

$$\Pr(Z > 4 \log(1/\delta)) \leq \delta^2. \quad (38)$$

The proximal operator is a strictly increasing function of Z , so we can determine the bound on its tail by determining an upper bound on $\text{Prox}_{a\rho/\delta} \left(\frac{4b \log(1/\delta)}{\sqrt{\delta}} \right)$. The first-order optimality condition for the proximal operator is

$$w^* = \frac{4b \log(1/\delta)}{\sqrt{\delta}} - \frac{a}{\delta} \rho'(w^*). \quad (39)$$

It is clear that for sufficiently small δ , $w^* < 0$, since $\rho'(u) \geq 1/2$ for $u \geq 0$. Therefore, since $\rho'(u) = e^u / (1 + e^u)$, there exists $c_\delta \in (1/2, 1)$ such that $\rho'(w^*) = c_\delta e^{w^*}$. We can then solve for and bound w^* for some $c > 0$ and sufficiently small δ as

$$w^* = \frac{4b \log(1/\delta)}{\sqrt{\delta}} - W_0 \left(\frac{ac_\delta}{\delta} \exp \left(\frac{4b \log(1/\delta)}{\sqrt{\delta}} \right) \right) \quad (40)$$

$$\leq -\log \left(\frac{ac_\delta}{\delta} \right) + \log \left(\frac{4b \log(1/\delta)}{\sqrt{\delta}} + \log \left(\frac{ac_\delta}{\delta} \right) \right) \quad (41)$$

$$\leq \log(c\delta \log(1/\delta)), \quad (42)$$

where W_0 is the principal branch of the Lambert W function, and the first inequality follows from the lower bound $W_0(x) \geq \log x - \log \log x$ for $x \geq e$. Let δ_0 be a sufficiently small so that the above arguments hold, and the claim is proved. \square

Applying Lemma 6 with $a_0 = c_{\bar{\gamma}}$ and $b_0 = c_1$ to (30), we can use the facts that $\rho'(u) \leq 1$ and that $\rho'(u) \leq e^u$ to obtain for some $c_r > 0$

$$r^2 \leq 2(c_r^2 \delta^2 \log^2(1/\delta) + \delta^2). \quad (43)$$

Thus for some $c_{\bar{r}} > 0$, $\bar{r} \leq c_{\bar{r}} \delta \log(1/\delta)$ for sufficiently small δ . We then apply Lemma 6 to (32) to similarly obtain for some $c_{\theta} > 0$

$$\theta \leq \frac{1}{2}(c_{\theta} \delta \log(1/\delta) + \delta^2) \quad (44)$$

Thus for some $c_{\bar{\theta}} > 0$, $\bar{\theta} \leq c_{\bar{\theta}} \delta \log(1/\delta)$ for sufficiently small δ . Therefore, returning again to (35), there exists some $c_2 > 0$ such that for sufficiently small δ ,

$$\kappa^2 \bar{\alpha}^2 + \bar{\sigma}^2 \leq c_2^2 \delta \log^2(1/\delta). \quad (45)$$

Hence the output variance tends to zero as $\delta \rightarrow 0^+$.

D.1.3 Membership inference advantage

We wrap up the proof by proposing two more lemmas for the proximal operator of the logistic loss

Lemma 7. Fix $C > 0$. For all v such that $|v| < C$ and $y \in \{0, 1\}$,

$$\lim_{a \rightarrow \infty} |\text{Prox}_{a\ell(y, \cdot)}(v)| = \infty \text{ uniformly}, \quad (46)$$

where $\ell(y, z) = \log(1 + \exp(z)) - yz$ is the logistic loss.

Proof. The proximal operator $\text{Prox}_{a\ell(y, \cdot)}(v)$ is the unique solution $w \in \mathbb{R}$ to the equation

$$w = v + a(y - \rho'(w)). \quad (47)$$

Consider $y = 1$, and suppose the claim was not true. Then there exists $c_1 > 0$ such that for all $a_0 > 0$, there exists $a > a_0$ and $v \in (-C, C)$ such that $|w| < c_1$. Let $c_2 = \rho'(c_1)$. This implies that

$$c_1 + ac_2 > v + a. \quad (48)$$

Since $c_2 < 1$, this inequality does not hold for any $a > a_0$ if a_0 is sufficiently large, leading to a contradiction. The case for $y = 0$ is entirely analogous if we make the substitution $\rho'(w) = 1 - \rho'(-w)$. \square

Lemma 8. Let Z be a standard normal random variable. Then for any $\tau > 0$, if a_n and b_n are sequences such that as $n \rightarrow \infty$, $a_n \rightarrow \infty$ and $b_n \rightarrow 0$, then

$$\lim_{n \rightarrow \infty} \Pr(|\text{Prox}_{a_n \ell(y, \cdot)}(b_n Z)| > \tau) - \Pr(|b_n Z| > \tau) = 1, \quad (49)$$

Proof. For sufficiently large n , by a standard tail bound for Gaussian variables, with probability at least $1 - e^{-(\tau/b_n)^2/2}$, we know that $|b_n Z| < \tau$. Again for sufficiently large n , we know that $|\text{Prox}_{a_n \ell(y, \cdot)}(b_n Z)| > \tau$ for all $|b_n Z| < \tau$ by Lemma 7. Thus,

$$\Pr(|\text{Prox}_{a_n \ell(y, \cdot)}(b_n Z)| > \tau) - \Pr(|b_n Z| > \tau) \geq 1 - 2e^{-(\tau/b_n)^2/2}, \quad (50)$$

which tends to 1 as $n \rightarrow \infty$. \square

Applying Lemma 8 to our problem, using the fact that $\bar{\gamma} \rightarrow \infty$ and $\kappa^2 \bar{\alpha}^2 + \bar{\sigma}^2 \rightarrow 0$, we see that any adversary that applies a threshold $|\hat{f}(\mathbf{x})| > \tau$ for a fixed threshold τ will achieve MI advantage of 1 as $\delta \rightarrow 0$. Any loss-based fixed-threshold adversary inherits this behavior, as for the logistic loss, $\ell(y, \hat{f}(\mathbf{x}))$ is a monotonically decreasing function of $|\hat{f}(\mathbf{x})|$, so thresholding the loss is equivalent to thresholding the magnitude of the model output.

D.2 Part (b): test accuracy for the bi-level ensemble

In the bi-level ensemble, when applying Theorem 3 for $\tilde{\beta}^*$ in place of β^* , asymptotically, the first three equations in the nonlinear system (10) become

$$\begin{cases} \kappa^2 \alpha = \frac{\sigma \tau \theta \kappa^2}{1 + \frac{\lambda \sigma \tau}{\phi}}, \\ \gamma = \frac{\sigma \tau}{\delta} \left(\frac{1}{\phi + \lambda \sigma \tau} + \frac{\phi - 1}{\phi + \frac{\lambda \sigma \tau}{\eta} (\phi - 1)} \right), \\ \kappa^2 \alpha^2 + \sigma^2 = \frac{(\sigma \tau \theta \phi \kappa)^2 + (\sigma \tau r)^2 \frac{\phi}{\delta}}{(\phi + \lambda \sigma \tau)^2} + \frac{(\sigma \tau r)^2 \frac{\phi}{\delta} (\phi - 1)}{(\phi + \frac{\lambda \sigma \tau}{\eta} (\phi - 1))^2}. \end{cases} \quad (51)$$

As we discussed in the proof of part (a), r and θ are always upper bounded by constants, so as $\lambda \rightarrow \infty$, regardless of the behavior of $\sigma \tau$, the left-hand sides of all three equations tend to zero. For this reason, applying our reformulations of the proximal operators and taking appropriate limits, the last three equations in the nonlinear system become

$$\begin{cases} r^2 = \frac{1}{4}, \\ \theta = \mathbb{E} [\rho''(-\kappa Z_1)], \\ \sigma \tau = 4. \end{cases} \quad (52)$$

These simplifications largely result from applying $\rho'(0) = 1/2$ and appealing to symmetry arguments. The final equation results from the algebraic manipulation

$$\frac{\gamma}{\sigma \tau} = \mathbb{E} \left[2\rho'(-\kappa Z_1) \left(1 - \frac{1}{1 + \gamma \rho''(\text{Prox}_{\gamma \rho}(\kappa \alpha Z_1 + \sigma Z_2))} \right) \right] \quad (53)$$

$$= \mathbb{E} \left[2\rho'(-\kappa Z_1) \frac{\gamma \rho''(\text{Prox}_{\gamma \rho}(\kappa \alpha Z_1 + \sigma Z_2))}{1 + \gamma \rho''(\text{Prox}_{\gamma \rho}(\kappa \alpha Z_1 + \sigma Z_2))} \right]. \quad (54)$$

Now knowing that $\bar{\sigma} \bar{\tau} = 4$, we can consider very large $\lambda \rightarrow \infty$ to obtain

$$\begin{cases} \alpha = \frac{\theta \phi}{\lambda} + o\left(\frac{1}{\lambda}\right), \\ \gamma = \frac{2}{\lambda \delta} + o\left(\frac{1}{\lambda}\right), \\ \kappa^2 \alpha^2 + \sigma^2 = \frac{1}{\lambda^2} \left((\theta \phi \kappa)^2 + \frac{\phi}{4\delta} \left(1 + \frac{\eta^2}{\phi - 1} \right) \right) + o\left(\frac{1}{\lambda}\right). \end{cases} \quad (55)$$

Generalization error equals $\Pr(y \oplus \mathbb{1}\{\mathbf{x}^\top \hat{\beta} > 0\}) = 1$, where \oplus is the exclusive or operator, which by symmetry we can compute as

$$\Pr(y \oplus \mathbb{1}\{\mathbf{x}^\top \hat{\beta} > 0\}) = 2 \Pr(y = 0, \bar{\alpha} \mathbf{x}^\top \beta^* + \bar{\sigma} Z > 0) \quad (56)$$

$$= 2 \mathbb{E}_{\mathbf{x}} \left[\Pr(y = 0 | \mathbf{x}^\top \beta^*) \Phi \left(\frac{\mathbf{x}^\top \beta^*}{\bar{\sigma} / \bar{\alpha}} \right) \right], \quad (57)$$

where $\Phi: \mathbb{R} \rightarrow [0, 1]$ is the standard normal CDF, and Z is a standard normal random variable. It can be shown that this is decreasing in α/σ , and from the above, in the limit as $\lambda \rightarrow \infty$,

$$\frac{\bar{\alpha}^2}{\bar{\sigma}^2} = \frac{4\theta^2 \frac{\phi}{\delta}}{1 + \frac{\eta^2}{\phi - 1}}, \quad (58)$$

which is increasing in ϕ for fixed $d/n = \delta/\phi$.

E Membership advantage for the bi-level ensemble

We know from the previous section, Theorem 4, and Theorem 3 that the predictions on training and test points follow

$$\mathbf{x}_i^\top \widehat{\boldsymbol{\beta}} \xrightarrow{d} \text{Prox}_{\bar{\gamma}\ell(y_i, \cdot)}(\bar{\alpha}Z_i + \bar{\sigma}W), \quad \mathbf{x}^\top \widehat{\boldsymbol{\beta}} \xrightarrow{d} \bar{\alpha}Z + \bar{\sigma}W, \quad (59)$$

where $\mathbf{x}_i^\top \boldsymbol{\beta}^* \xrightarrow{d} Z_i$, $\mathbf{x}^\top \boldsymbol{\beta}^* \xrightarrow{d} Z$, and $W \sim \mathcal{N}(0, 1)$ is independent of Z_i or Z . Here randomness is over the training dataset, so for a fixed $\boldsymbol{\beta}^*$ and \mathbf{x}_i (or \mathbf{x}), we have a fixed Z_i (or Z). Suppose the adversary is given some \mathbf{x}' and its (noisy) training label y' . If \mathbf{x}' (with corresponding Z') is *not* a training point,

$$\mu_{\text{test}}(\hat{z}|\mathbf{x} = \mathbf{x}', y = y') = \mu_{\text{test}}(\hat{z}|\mathbf{x} = \mathbf{x}') \quad (60)$$

$$= \mu_W\left(\frac{\hat{z} - \bar{\alpha}Z'}{\bar{\sigma}}\right) \frac{1}{\bar{\sigma}}. \quad (61)$$

The first equality is from the independence of the model output and the unused training label, and the second equality comes by the change of variables formula for scalar random variables in terms of μ_W , which is a standard normal Gaussian density.

If \mathbf{x}' is a training point, we have the following probability density:

$$\mu_{\text{train}}(\hat{z}|\mathbf{x} = \mathbf{x}', y = y') = \mu_W\left(\frac{g_y(\hat{z}) - \bar{\alpha}Z'}{\bar{\sigma}}\right) \frac{g'_y(\hat{z})}{\bar{\sigma}}. \quad (62)$$

Here $g_y(\cdot)$ is the inverse of $\text{Prox}_{\bar{\gamma}\ell(y, \cdot)}(\cdot)$, which by the first-order optimality condition is

$$g_y(z) = z + \bar{\gamma}(\rho'(z) - y), \quad g'_y(z) = 1 + \bar{\gamma}\rho''(z). \quad (63)$$

We remind the reader that $\rho''(z) = \rho'(z)(1 - \rho'(z))$. Therefore, the densities can be easily evaluated by numerical integration.

Since the adversary is given the value of the loss, which is monotonic in $\hat{f}(\mathbf{x}')$, and knows predicted label $\hat{y}(\mathbf{x}')$, the adversary is equivalent to an adversary based on $\hat{f}(\mathbf{x}')$ with the densities described above. The optimal adversary is given by

$$A^*(f, \mathbf{x}', y') = \mathbb{1}\left\{\mu_{\text{train}}(\hat{f}(\mathbf{x}')|\mathbf{x} = \mathbf{x}', y = y') > \mu_{\text{test}}(\hat{f}(\mathbf{x}')|\mathbf{x} = \mathbf{x}', y = y')\right\}, \quad (64)$$

and we can compute its MI advantage specific to (\mathbf{x}', y') as

$$\text{Adv}(A^*, \hat{f}; \mathbf{x}', y') = \int_{\mathbb{R}} \max\{\mu_{\text{train}}(z|\mathbf{x} = \mathbf{x}', y = y') - \mu_{\text{test}}(z|\mathbf{x} = \mathbf{x}', y = y'), 0\} dz. \quad (65)$$

$$(66)$$

We can numerically evaluate this integral, and then we can compute the average sample-specific membership inference advantage as

$$\text{Adv}(A^*, \hat{f}) = \mathbb{E}_{\mathbf{x}', y'} \left[\text{Adv}(A^*, \hat{f}; \mathbf{x}', y') \right], \quad (67)$$

which we can easily compute by numerical integration over the Gaussian density of Z' and the fact that $\Pr(y' = 1|\mathbf{x}') = \rho'(Z')$.

F Train vs. test distribution simulation

To validate our derivation of the sample-specific output distribution, we compute empirical histograms over many trials for fixed data points and labels. See Figure 7.

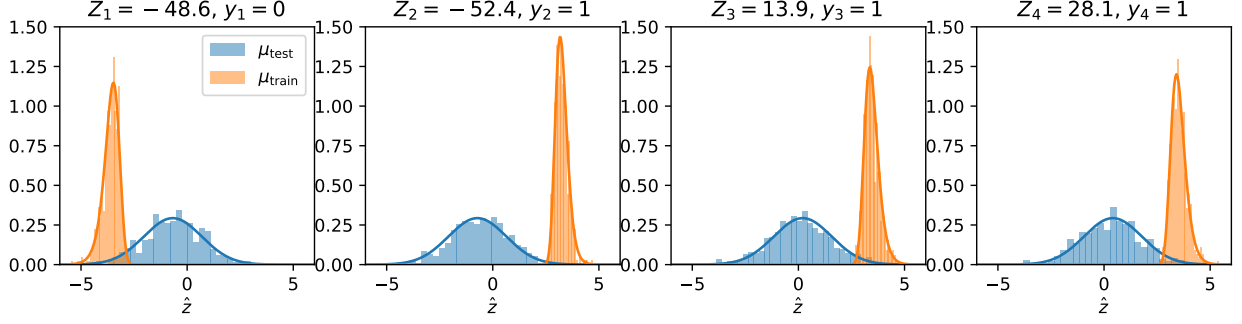


Figure 7: Theoretical densities (solid line) versus empirical histograms of sample-specific output distributions when \mathbf{x}' is a test (blue) or training (orange) training point. For each training sample (\mathbf{x}_i, y_i) , $i \in \{1, 2, 3, 4\}$, we plot the corresponding theoretical densities $\mu_{\text{test}}(\hat{z}|\mathbf{x}' = \mathbf{x}_i, y' = y_i)$ and $\mu_{\text{train}}(\hat{z}|\mathbf{x}' = \mathbf{x}_i, y' = y_i)$ as described in Appendix E given $Z_i = \mathbf{x}_i^\top \beta^*$ for a bi-level ensemble with $n/d = 1/2$, $\phi = 3$, $\sigma_\beta = 50$, $\lambda = 0.1$, $\eta = 1$. The histograms are of the outputs over 500 trials where $n = 500$ additional training points are used to train a logistic regression model on bi-level ensemble features either including or not including (\mathbf{x}_i, y_i) . Thus even for problems of real data sizes, the theory matches empirical results.

G Experimental setups

This section provides details on the experimental setups for sections 3.1, 3.3, 4 and figures 2, 3, 4, 5, and 6.

G.1 SVM experimental setup

This subsection provides details on the SVM experiments whose results are shown in Figure 2. For all SVM models, we use scikit-learn’s SVC class [50]. When the number of SVM parameters is smaller than the number of data points in the training dataset, we add regularization $C = 1$, where C is the corresponding regularization parameter in scikit-learn’s SVC class. Else, we use $C = 10^{20}$, essentially applying no regularization to yield the hard-margin SVM. The hard-margin SVM has been studied considerably in the double descent literature [15, 45], especially with regards to its relationship to logistic regression trained with gradient descent [51, 52].

We use the optimal MI adversary [22], which is a likelihood ratio test, as our MI attack. Suppose we are given two discrete distributions over values s_i with probability mass functions $q_{m=0}$ and $q_{m=1}$. The optimal adversary A^* is defined by:

$$A^*(s_i) = \begin{cases} 1 & \text{if } q_{m=1}(s_i) > q_{m=0}(s_i), \\ 0 & \text{otherwise} \end{cases}. \quad (68)$$

For each experiment, the general procedure is as follows. We first generate a D -dimensional data point \mathbf{x}_0 with binary label y_0 , for some D . This is the data point on which MI will be performed. Then, for an integer p , we perform the following procedure L times. We first generate an $n \times p$ training dataset matrix \mathbf{X} , for some n , and a corresponding label vector \mathbf{y} . Generally, these are distributed in the same way as (\mathbf{x}_0, y_0) . All experiments here are binary classification tasks, so $\mathbf{y}_i \in \{-1, +1\}$ for $i \in \{1, 2, \dots, n\}$. We then apply label noise to \mathbf{y} : we flip each label \mathbf{y}_i to the other class with probability α . Afterwards, we learn an SVM on \mathbf{X} and \mathbf{y} . We then denote by \hat{y}_0 the signed distance of \mathbf{x}_0 to the decision hyperplane of the learned SVM. We collect the \hat{y}_0 of all L learned SVMs into an output vector $\hat{\mathbf{y}}_{m=0}$. We then repeat the same procedure another L times, but this time, before learning the SVM on \mathbf{X} and \mathbf{y} , we first replace the first rows $\mathbf{X}_1 = \mathbf{x}_0$ and $\mathbf{y}_1 = y_0$. Label noise is never applied to y_0 . We collect the resulting L signed distances to the learned SVM hyperplanes into the output vector $\hat{\mathbf{y}}_{m=1}$. We form discrete histograms for both $\hat{\mathbf{y}}_{m=0}$ and $\hat{\mathbf{y}}_{m=1}$ with bin width b . Finally, we perform the optimal adversary attack on these histograms and measure the corresponding membership advantage. This entire experiment is repeated for multiple values p to generate Figure 2.

The following subsections provide the distributions of \mathbf{x}_0 , y_0 , \mathbf{X} , and \mathbf{y} , as well as the hyperparameters n (number of data points), D (full data dimensionality), label noise probability α , L (number of samples used

to form the histogram), histogram bin width b , and the set of number of features p investigated for each data model.

G.1.1 Weak features

The weak features experiment is based on the weak features ensemble discussed in Definition 9 of [15]. In our experiment, we let $D = 1000$, $\mathbf{x}_0 \sim \mathcal{N}(\mathbf{1}_D, \mathbf{I}_D)$, and $y_0 = 1$. We perform the experiment for $p \in \{5, 10, 15, \dots, 95, 100, 200, 300, \dots, 900\}$ with number of data points $n = 100$, number of samples $L = 20,000$, histogram bin width $b = 0.05$, and label noise probability $\alpha = 0.2$. The $n \times p$ training dataset matrix \mathbf{X} is generated such that the i 'th row $\mathbf{X}_i \sim \mathcal{N}(z_i, \mathbf{I}_p)$, with $z_i \sim \mathcal{N}(0, 1)$. The elements of the label vector \mathbf{y} are defined by $y_i = \text{sign}(z_i)$. In essence, each element of a training data point \mathbf{X}_i is the true signal z_i (on which the label y_i is based) corrupted by Gaussian noise.

G.1.2 Separable Gaussians

The separable Gaussians model is based on synthetic dataset 1 of [44] with some modifications. In our experiment, we set $D = 1000$ and generate \mathbf{x}_0 by sampling its individual elements as:

$$\mathbf{x}_{0,j} \sim \begin{cases} \mathcal{N}(1, 1) & \text{if } j \leq 100 \\ \mathcal{N}(0, 1) & \text{otherwise} \end{cases}, \quad (69)$$

with true label $y_0 = 1$. We perform the experiment for $p \in \{10, 20, 30, \dots, 90, 100, 150, 200, 250, \dots, 1000\}$ with number of data points $n = 100$, number of samples $L = 10,000$, and histogram bin width $b = 0.05$. Each element of the label vector \mathbf{y}_i is randomly selected from $\{-1, +1\}$ with uniform probability. The individual elements (row i and column j) of the training dataset matrix \mathbf{X} are distributed as:

$$\mathbf{X}_{i,j} \sim \begin{cases} \mathcal{N}(\mathbf{y}_i, 1) & \text{if } j \leq 100 \\ \mathcal{N}(0, 1) & \text{otherwise} \end{cases}. \quad (70)$$

Label noise with probability $\alpha = 1$ is then applied to \mathbf{y} after \mathbf{X} is generated. Essentially, the first $\min(100, p)$ features of each data point depend on its true class, and the remaining features are irrelevant (independent of the class). Thus, in the overparameterized regime, as p increases, we are including more irrelevant features to the model.

G.1.3 Random ReLU features

The random ReLU features model has been studied by multiple papers, such as [45] (section 3) and [53]. In essence, it is a two-layer ReLU neural network with fixed first-layer random weights. Different from the previous SVM data models, here \mathbf{x}_0 is defined differently for each trained SVM model because of the random projections. Instead, there is a latent data vector \mathbf{z}_0 that is kept fixed for all experiments and on which MI is performed. We set $D = 200$, and generate \mathbf{z}_0 by sampling it from $\mathcal{N}(0, \mathbf{I}_D)$. We perform the experiment for $p \in \{10, 20, 30, \dots, 90, 100, 150, 200, \dots, 950\}$ with number of data points $n = 100$, number of samples $L = 100,000$, histogram bin width $b = 0.001$, and no label noise. To generate the training data, a random $p \times D$ "featurizer" matrix \mathbf{W} is first generated by sampling each row independently from the D -dimensional unit sphere. Then, an $n \times D$ feature data matrix \mathbf{Z} is generated by sampling each element iid standard normal. The training data matrix $\mathbf{X} = \max(0, \mathbf{Z}\mathbf{W}^T)$, where the max operation is applied elementwise. The MI data point x_0 is defined as $x_0 = \max(0, \mathbf{z}_0^T \mathbf{W}^T)$. Note that since \mathbf{W} is sampled for each trained SVM, \mathbf{x}_0 changes for each experimental run. To generate the labels of the data points, first, a random vector β is sampled uniformly from the D -dimensional sphere of radius 4 (such that $\|\beta\|_2 = 4$). Then, y_i is assigned class 1 with probability $\frac{1}{1+e^{-\mathbf{z}_i^T \beta}}$ and class -1 otherwise. The label y_0 of x_0 is defined similarly and is assigned class 1 with probability $\frac{1}{1+e^{-\mathbf{z}_0^T \beta}}$ and class -1 otherwise. Essentially, the class of a data point depends only on \mathbf{Z} , and the training set consists of random projections of \mathbf{Z} that are then passed through the ReLU operation.

G.1.4 CIFAR10

To experiment on real data, we train SVMs on random projections of a subset of the CIFAR10 dataset [46]. We first define \mathbf{z}_0 to be the first image of the training dataset with class “airplane” converted to grayscale and then vectorized. We perform the experiment for $p \in \{10, 20, 30, \dots, 90, 100, 200, 300, \dots, 1800, 1900\}$ with number of data points $n = 200$, number of samples $L = 10,000$, histogram bin width $b = 0.05$, and no label noise. To generate the $n \times p$ data matrix, we first randomly sample $\frac{n}{2}$ images uniformly from the “airplane” images of the dataset (excluding \mathbf{x}_0) and $\frac{n}{2}$ images from the “automobile” images of the dataset. We convert the images to grayscale, vectorize them, and collect them into a matrix \mathbf{Z} (where each row is a vectorized image). Since each image is of size 32×32 , the vectorized image is $D = 1024$ dimensional. We then sample a $p \times 1024$ random projections matrix \mathbf{W} , where each row is sampled uniformly from the 1024-dimensional unit sphere. Finally, the data matrix $\mathbf{X} = \mathbf{Z}\mathbf{W}^\top$. The MI point $\mathbf{x}_0 = \mathbf{z}_0^\top \mathbf{W}^\top$. The labels of each data point is -1 if it originated from an “airplane” image and $+1$ if it originated from an “automobile” image.

G.2 Neural network experimental setup

This subsection provides details on the NN experiments whose results are shown in Figures 3, 4, 5, and 6. Unless otherwise specified, we use the default hyperparameters and initializations of Pytorch implementations. The NN experiments are run on our internal servers with the following GPUs: NVIDIA TITAN X (Pascal), NVIDIA GeForce RTX 2080 Ti, NVIDIA TITAN RTX, and NVIDIA A100. The choice of which particular GPU is used for each experiment is decided only based on availability of the GPUs in our internal servers.

G.2.1 The MI attack

The MI attack employed in these experiments is the loss-threshold attack [30, 19, 41]. Given a trained NN f , the data point of interest $\mathbf{z}_0 = (\mathbf{x}_0, y_0)$, and a loss function ℓ , the prediction $A(f(\mathbf{x}_0), \mathbf{z}_0)$ of this attack is given by:

$$A(f(x_0), y) = \begin{cases} 1 & \text{if } \ell(y_0, f(\mathbf{x}_0)) < \tau_{\mathbf{z}_0}, \\ 0 & \text{otherwise} \end{cases}, \quad (71)$$

where $\tau_{\mathbf{z}_0}$ is a calibrated threshold. The threshold is learned with the following procedure. Given a full training dataset \mathcal{D} , we train n_{shadow} shadow models on random subsamples of this dataset such that for each \mathbf{z}_0 in the full dataset, some models are trained on datasets including \mathbf{z}_0 and the rest are trained on datasets that do not include \mathbf{z}_0 . The shadow models have the same architecture and training procedure as the target models that will be attacked. Let $n_{\text{shadow}, \mathbf{z}_0, m=1}$ and $n_{\text{shadow}, \mathbf{z}_0, m=0}$ denote the (random) numbers of shadow models trained on \mathbf{z}_0 and not trained on \mathbf{z}_0 , respectively. We then evaluate all these shadow models on \mathbf{z}_0 and collect all loss values of the shadow models trained on \mathbf{z}_0 into a vector $\mathbf{s}_{\mathbf{z}_0, m=1}$ and the loss values of the shadow models not trained on \mathbf{z}_0 into a vector $\mathbf{s}_{\mathbf{z}_0, m=0}$. The membership advantage $\text{Adv}_{\text{shadow}}$ of a threshold $\hat{\tau}_{\mathbf{z}_0}$ is given by:

$$\text{Adv}_{\text{shadow}, \mathbf{z}_0} = \frac{|\{s \in \mathbf{s}_{\mathbf{z}_0, m=1} : s < \tau_{\mathbf{z}_0}\}|}{n_{\text{shadow}, \mathbf{z}_0, m=1}} - \frac{|\{s \in \mathbf{s}_{\mathbf{z}_0, m=0} : s < \tau_{\mathbf{z}_0}\}|}{n_{\text{shadow}, \mathbf{z}_0, m=0}}, \quad (72)$$

which is simply the difference of the empirical true positive rate and false positive rate. Note that there are many optimal thresholds that maximize $\text{Adv}_{\text{shadow}}$. Indeed, if $\hat{\tau}_{\mathbf{z}_0}$ is one such optimal threshold, then so is any $\tau \in [s_{m=1}^*, s_{m=0}^*]$, where $s_{m=1}^*$ is the closest element in $\mathbf{s}_{m=1}$ that is less than $\tau_{\mathbf{z}_0}$ and $s_{m=0}^*$ is the closest element in $\mathbf{s}_{m=0}$ that is greater than $\tau_{\mathbf{z}_0}$. Thus, we set the attack’s calibrated loss threshold as the midpoint: $\tau_{\mathbf{z}_0} = \frac{1}{2}(s_{m=1}^* + s_{m=0}^*)$. This sample-based loss threshold attack, wherein a different threshold is learned for each data point \mathbf{z}_0 , is the attack we use for the CIFAR10 and Multi30k experiments.

A variation of this attack that we apply for the Purchase100 dataset is the global loss threshold, where $\tau_{\mathbf{z}_0} = \tau$ for every \mathbf{z}_0 . In words, the same threshold value is applied when attacking the model on any data point. The procedure for threshold calibration is the same, except now $\mathbf{s}_{m=1}$ contains the losses for each of the data points each model was trained on and $\mathbf{s}_{m=0}$ contains the losses for the data points the models were not trained on.

G.2.2 Evaluation procedure

To evaluate the attack, we first randomly subsample a training dataset \mathcal{S} from the full training dataset \mathcal{D} and train a target model on \mathcal{S} . Denote by $\bar{\mathcal{S}}$ the data points in \mathcal{D} that are not in \mathcal{S} . We collect the losses of the target model on each data point in \mathcal{S} into a vector $\mathbf{t}_{m=1}$ and the losses of the target model on each data point in $\bar{\mathcal{S}}$ into a vector $\mathbf{t}_{m=0}$. The membership advantage for the target model is:

$$\text{Adv}_{\text{target}} = \frac{|\{t \in \mathbf{t}_{m=1} : t < \tau_{z_0}\}|}{|\mathcal{S}|} - \frac{|\{t \in \mathbf{t}_{m=0} : t < \tau_{z_0}\}|}{|\bar{\mathcal{S}}|}. \quad (73)$$

We repeat this evaluation procedure n_{target} times, each time training a new target model on a newly sampled \mathcal{S} . The mean and standard deviation of the membership advantage over all experimental runs is what is reported in the paper figures.

Each shadow and target model is trained for E epochs with checkpoints saved every C epochs, where E and C differ per dataset. For the experiments in Section 3.1 and Figure 3, the checkpoints for each shadow and target model that achieves the highest classification accuracy rate on the dataset’s validation set is used for the experiment. The results in Figures 4 and 5 are obtained for each checkpoint. For each curve in Figure 6, for all shadow and target models, we use the same number of epochs: the number of epochs (out of the checkpoints acquired) that achieves a membership advantage (Figure 6a) or test error (6b) closest to the one specified in the figure.

G.2.3 Datasets and architectures

We split each dataset into a “full training dataset” and a validation set. The full training dataset contains all the point son which membership inference will be performed. Each shadow and target model will be trained on a sample of the full training dataset such that the full training dataset would always contain both members (training points) and non-members (test points) for each model. The validation set is only used for calculating classification test error.

Classification on Purchase100. The Purchase100 dataset is based on Kaggle’s “acquire valued shoppers” challenge dataset subsequently processed by [13]. It contains 197,324 length-600 binary feature vectors, each belonging to 1 of 100 classes. Each feature vector corresponds to a purchaser, and each entry of the vector corresponds to whether or not a particular product was purchased by the customer. The 100 classes correspond to purchasing styles. We use the first 180,000 data points as the full training dataset and the remaining data points for the validation set. We train two-layer neural networks with hidden dimension w , which we vary. We set $n_{\text{shadow}} = 80$ and $n_{\text{target}} = 20$. Each model is trained on a random sample of 10,000 data points. We use the ADAM optimizer [54] with a learning rate of 0.001 for $E = 3000$ epochs with checkpoints saved every $V = 20$ epochs. For Figure 5, we save checkpoints every $V = 1$ epoch and only display the results for less than 3000 epochs for better visualization (each curve uses a different number of epochs, according to which provides best visualization).

Image classification on CIFAR10. The CIFAR10 dataset [46] contains 60,000 32×32 RGB images, each belonging to 1 of 10 object classes. We use the 50,000 images in the official training dataset as our full training dataset, and the 10,000 images in the official validation dataset as our validation set. We train ResNet18 models [47] to perform image classification on the dataset. To vary the models’ widths, we follow [5] and use convolutional layer widths (number of filters) of $[w, 2w, 4w, 8w]$ for different w values. Note that $w = 64$ yields the original ResNet18 architecture. We set $n_{\text{shadow}} = 50$ and $n_{\text{target}} = 50$, where each model is trained on a random sample of 25,000 images. We train for 50,000 gradient steps using the ADAM optimizer [54] with a batch size of 128 (amounting to ≈ 256 epochs through the training dataset), a learning rate of 0.0001 and the cross-entropy loss. Data augmentation is a common technique used in image classification, and so we also employ random translations of up to 4 pixels and random horizontal flipping during training, as was done by [5].

Language translation on Multi30K. The Multi30K dataset [48] consists of 29,001 pairs of English-German sentences. We perform English to German translation on these sentences using the Transformer architecture [49]. To vary the models’ widths, we follow [5] and set the encoder/decoder feature sizes to w and the fully connected layers’ dimensions to $4w$ for different values of w . We train for 300 epochs using the ADAM optimizer [54] with a learning rate of 0.0001, a batch size of 128, and the cross-entropy loss over each token. We set $n_{\text{shadow}} = 8$ and $n_{\text{target}} = 2$ and train each model on a random sample of 14,500 sentence pairs.

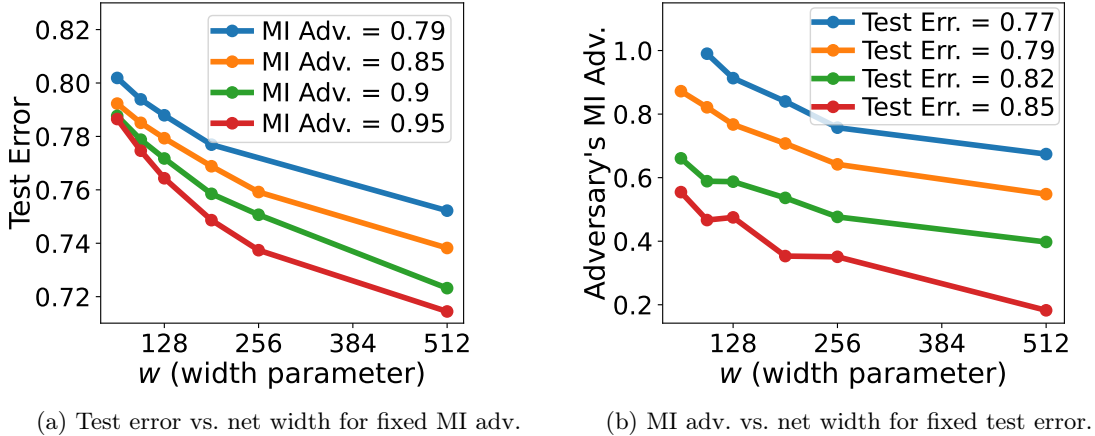


Figure 8: **Overparameterization with early stopping eliminates the privacy–utility trade-off on Multi30k.** This is similar to Figure 6 in the main body, but performed on the Multi30k dataset with the Transformer architecture. (a) For each network width, we train the network until it reaches a given MI advantage value. We then plot the test error of the networks. Observe how test error decreases with parameters at a fixed MI advantage value. Thus, this eliminates the privacy–utility trade-off. Proper tuning of parameters and epochs together improves model accuracy without damaging its privacy. (b) Same as (a) but switching the roles of MI advantage and test error.

In calculating the loss of a sentence pair for performing membership inference, we sum the cross-entropy loss values over all tokens in the sentence and divide by the sentence length.

H Additional Experiments

In Figure 8, we show the equivalent of Figure 6 in the main paper for the transformer architecture on the Multi30k dataset. Similarly to the Purchase100 and CIFAR10 datasets, increasing the width of the neural network here improves either privacy (i.e. decreases membership advantage) or test accuracy when holding the other fixed via proper epoch tuning.

In Figures 3, 4, 5, and 6, we used the sample-specific loss threshold attack for CIFAR10 and Multi30K, where a different loss threshold is learned for each data point. Here, we repeat the same experiments using the global loss threshold, where a single threshold value is used for all the data points. Note that in the mentioned figures, we already employed the global loss threshold attack for Purchase100. The trends we observe for the global loss threshold attack are similar to those of the sample-specific loss threshold attack. The results are shown in Figures 9, 10, 11, and 12. We use $n_{\text{shadow}} = n_{\text{target}} = 15$ for both datasets in this experiment. Ultimately, we demonstrate that all our observed empirical phenomena on the relationships of parameters, training epochs, membership inference, and test error are robust across different MI attacks.

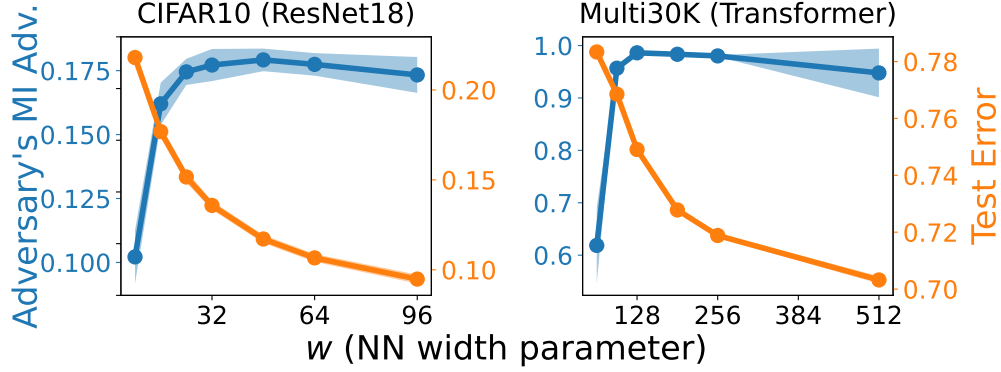


Figure 9: **Privacy vs. parameters (global loss threshold attack)**. We repeat the experiment in Figure 3, but now using the global (instead of sample-specific) loss threshold attack. Similarly, as the number of network parameters increases, membership advantage increases while test error decreases.

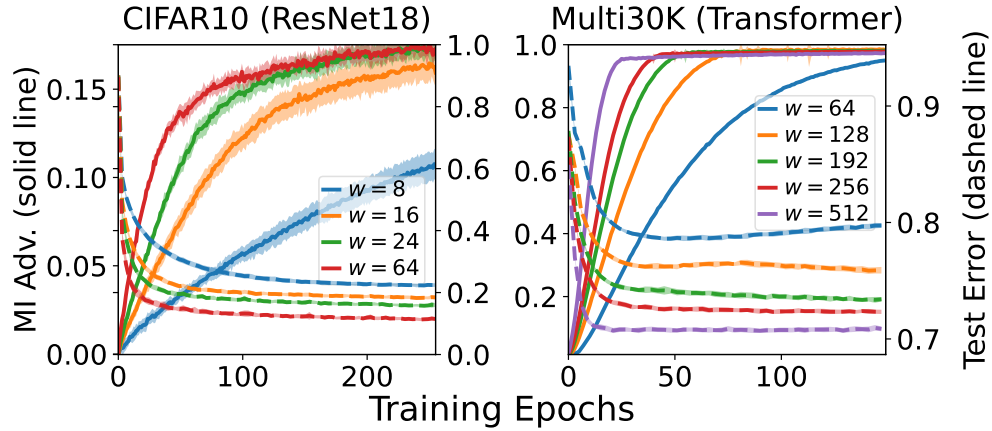


Figure 10: **Privacy vs. epochs (global loss threshold attack)**. We repeat the experiment in Figure 4, but now using the global (instead of sample-specific) loss threshold attack. Again, as epochs increase, membership advantage increases while test error decreases.

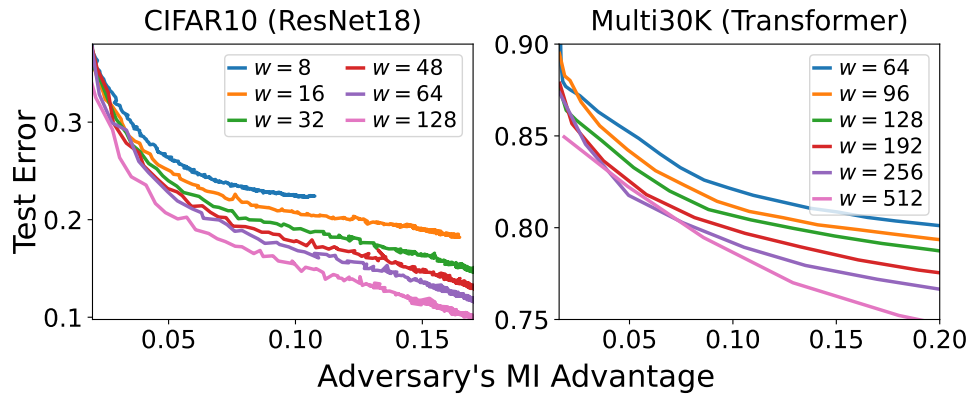


Figure 11: **Trade-offs (global loss threshold attack)**. We repeat the experiment in Figure 5, but now using the global (instead of sample-specific) loss threshold attack. We observe again how wider networks are closer to the lower-left portion of the graph, indicating better privacy and better test accuracy compared to their narrower counterparts.

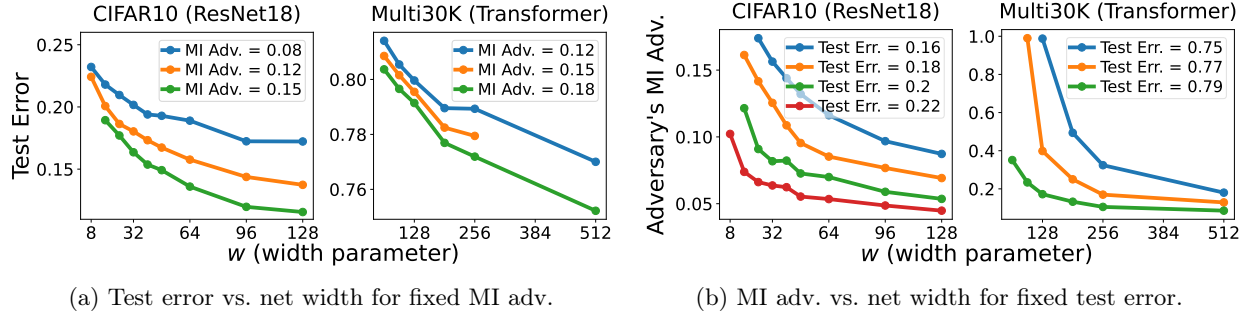


Figure 12: **Overparameterization with early stopping eliminates the privacy-utility trade-off (global loss threshold)**. Similar to Figures 6 and 8, but using the global loss threshold. Increasing the parameters can improve either privacy or test accuracy when keeping the other fixed (by epoch tuning).